REPUBLIC OF TÜRKİYE
ISTANBUL GELISIM UNIVERSITY
INSTITUTE OF GRADUATE STUDIES

Department of Civil Engineering

OPTIMIZATION FOR THE NATURAL FREQUENCIES OF FUNCTIONALLY GRADED BEAMS USING METAHEURISTIC ALGORITHMS

Master Thesis

Majed KANOUA

Supervisor

Asst. Prof. Dr. Ahmad Reshad Noori

Istanbul – 2025

THESIS INTRODUCTION FORM

Name and Surname : Majed KANOUA

Language of the Thesis : English

Name of the Thesis : Optimization For The Natural Frequencies of Functionally Graded Beams Using Metaheuristic Algorithms

Institute : Istanbul Gelişim University Institute of Graduate Studies

Department : CIVIL ENGINEERING

Thesis Type : Master

Date of the Thesis : 27/06/2025

Page Number : 70

Thesis Supervisors : Asst. Prof. Dr. Ahmad Reshad Noori

Index Terms : Functionally Graded Beams, Natural Frequency Optimization, Tug of War Optimization, Cyclical Parthenogenesis Algorithm, and Euler–Bernoulli Beam Theory.

Turkish Abstract : Makalede, kuvvet yasası sahip Euler-Bernoulli kiriş modeli, Halat Çekme Optimizasyonu (TWO) ve Döngüsel Partenogenez Algoritması (CPA) metasezgilerinin MATLAB uygulaması (kısıtlamalar için ceza fonksiyonları dahil) ve klasik sınır koşulları içinde yakınsama davranışını ve optimum frekans sonuçlarını karşılaştıran temel sonuçlar açıklanmaktadır.

Distribution List :

1. To the Institute of Graduate Studies of Istanbul Gelisim University
2. To the National Thesis Center of YÖK (Higher Education Council)

REPUBLIC OF TÜRKİYE
ISTANBUL GELISIM UNIVERSITY
INSTITUTE OF GRADUATE STUDIES

Department of Civil Engineering

OPTIMIZATION FOR THE NATURAL FREQUENCIES OF FUNCTIONALLY GRADED BEAMS USING METAHEURISTIC ALGORITHMS

Master Thesis

Majed KANOUA

Supervisor

Asst. Prof. Dr. Ahmad Reshad Noori

Istanbul – 2025

DECLARATION

I hereby declare that in the preparation of this thesis, scientific ethical rules have been followed, the works of other persons have been referenced in accordance with the scientific norms if used, there is no falsification in the used data, any part of the thesis has not been submitted to this university or any other university as another thesis.

Majed KANOUA

.../.../2025

TO ISTANBUL GELISIM UNIVERSITY

THE DIRECTORATE OF INSTITUTE OF GRADUATE STUDIES

The thesis study of Majed KANOUA titled as OPTIMIZATION FOR THE NATURAL FREQUENCIES OF FUNCTIONALLY GRADED BEAMS USING METAHEURISTIC ALGORITHMS has been accepted as MASTER/PhD THESIS in the department of Civil Engineering by our jury.

Director

Assist. Prof. Dr. Ali ETE

Member

Assist. Prof. Dr. Ahmad Reshad NOORI

(Supervisor)

Member

Assoc. Prof. Dr. Metin MEHMETOGLU

APPROVAL

I approve that the signatures above signatures belong to the aforementioned faculty members.

... / ... / 20..

Prof. Dr. İzzet GÜMÜŞ

Director of the Institute

SUMMARY

The thesis describes optimizing the lowest natural frequencies of functionally graded beams, which have varying material characteristics based on a power-law across thickness, using classical boundary conditions. The Euler-Bernoulli beam concept is expanded to include power-law distributions in each layer, resulting in spatially variable stiffness and mass density. Frequencies of free vibration expressed in closed form. To navigate the very non-convex design space defined by volume fraction gradation parameters and layer thickness ratios, MATLAB employs two metaheuristic techniques. The first is the Tug of War Optimization (TWO) algorithm, and the second is the Constrained Particle Algorithm (CPA), which uses swarm-inspired updates coupled with adaptive penalty functions to enforce mass targets and manufacturability constraints in the non-convex design space defined by layer thickness ratios and volume fraction gradation parameters. Extensive numerical studies in clamped-free, clamped-clamped, and simply supported cases show that CPA converges faster to high-quality solutions, achieving up to a 20% increase in the first natural frequency in preliminary runs, whereas TWO achieves even greater frequency enhancements (up to 25%) at the expense of longer runtimes. Sensitivity studies reveal that higher material gradients disproportionately increase stiffness, providing an effective tuning lever. Overall, CPA is suggested for quick design iterations and mass- or time-sensitive applications, whereas TWO is preferred when peak vibrational performance trumps computing cost. Future work will expand these algorithms to three-dimensional plates and shells, incorporate gradient-based local adjustments, and test optimal gradation profiles empirically using 3D-printed specimens.

Key Words: Functionally Graded Beams, Natural Frequency Optimization, Tug of War Optimization (TWO), Constrained Particle Algorithm (CPA), Euler–Bernoulli Beam Theory, Metaheuristic Algorithms, Volume Fraction Gradation

ÖZET

Bu tez, kalınlık boyunca bir güç kuralı (power-law) dağılımına sahip, malzeme özellikleri değişken olan fonksiyonel derecelendirilmiş kirişlerin (Functionally Graded Beams) en düşük doğal frekanslarının optimizasyonunu klasik sınır koşulları altında ele almaktadır. Euler-Bernoulli kiriş teorisi, her katmanda güç kuralı dağılımlarının eklenmesiyle genişletilmiş ve böylece mekânsal olarak değişen rijitlik ve kütle yoğunluğu ortaya çıkmıştır. Serbest titreşim frekansları kapalı formda ifade edilmiştir. Katman kalınlık oranları ve hacim oranı derecelendirme parametreleriyle tanımlanan son derece konkav olmayan tasarım uzayında yön bulmak amacıyla MATLAB, iki metasezgisel tekniği kullanmaktadır. Birincisi, Tug of War Optimization (TWO) algoritması; ikincisi ise, katman kalınlık oranları ve hacim oranı derecelendirme parametreleriyle tanımlanan konkav olmayan tasarım uzayında kütle hedeflerini ve üretilebilirlik kısıtlarını sağlamak için uyarlamalı ceza fonksiyonlarıyla desteklenen sürü esinli güncellemeler kullanan Constrained Particle Algorithm (CPA) algoritmasıdır. Ankastre-serbest, ankastre-ankastre ve basit mesnetli durumlarda yapılan kapsamlı sayısal incelemeler, CPA'nın yüksek kaliteli çözümlere daha hızlı yakınsadığını ve ön çalışmalar sırasında birinci doğal frekansta %20'ye kadar artış sağladığını göstermektedir. Öte yandan, TWO algoritması, daha uzun çalışma süreleri pahasına bile olsa %25'e kadar frekans iyileştirmeleri sağlamaktadır. Duyarlılık çalışmaları, daha yüksek malzeme gradyanlarının rijitliği orantısız şekilde artırdığını ve böylece etkin bir ayar kolu sağladığını ortaya koymuştur. Genel olarak, CPA hızlı tasarım yinelemeleri ve kütle veya zaman hassasiyeti olan uygulamalar için önerilirken, TWO algoritması ise titreşim performansının hesaplama maliyetinin önüne geçtiği durumlar için tercih edilmektedir. Gelecekteki çalışmalar, bu algoritmaların üç boyutlu plak ve kabuk yapılarına genişletilmesini, gradyan tabanlı yerel ayarlamaların entegrasyonunu ve optimum derecelendirme profillerinin 3B baskı örnekleriyle deneysel olarak test edilmesini hedeflemektedir.

Anahtar Sözcükler: Fonksiyonel Derecelendirilmiş Kirişler, Doğal Frekans Optimizasyonu, Tug of War Optimizasyonu (TWO), Kısıtlı Parçacık Algoritması (CPA), Euler–Bernoulli Kiriş Teorisi, Metasezgisel Algoritmalar, Hacim Oranı Derecelendirmesi

TABLE OF CONTENTS

SUMMARY ..... **i**
ÖZET ..... **ii**
TABLE OF CONTENTS ..... **iii**
ABBREVIATIONS ..... **v**
LIST OF TABLES ..... **vi**
LIST OF FIGURES ..... **viii**
PREFACE ..... **x**
INTRODUCTION **1**

CHAPTER ONE
PREVIOUS STUDIES

1.1. Previous studies 4

CHAPTER TWO
MATERIALS AND METHODS

2.1. Materials 10
2.2. Methods 12
2.2.1. CPA 14
2.2.2.TWO 15

CHAPTER THREE
RESULTS AND DİSCUSSİONS

3.1. Results obtained by CPA methods 16
3.2. Results obtained by TWO methods 20
3.3. Comparison between CPA and TWO results 25
3.4. Comparison between CPA and TWO results using Different Material Properties 41
3.4.1. First Material changing 41
3.4.2. The second material change 43
3.4.3. The third material change 45
3.4.4. The fourth material change 47

CHAPTER FOUR
CONCLUSION AND RECOMMENDATIONS

4.1. Conclusion and recommendations 49

REFERENCES 50

RESUME 54

ABBREVIATIONS

CPA	:	Cyclical Parthenogenesis Algorithm.
Eb	:	Effective Young's Modulus at the Bottom of the Beam.
Et	:	Effective Young's Modulus at the Top of the Beam.
FGM	:	Functionally Graded Material.
NIT, NT, s	:	Iterations.
Pb	:	Density at the Bottom of the Beam.
Pt	:	Density at the Top of the Beam.
TWO	:	Tug of War Optimization.
ω, W	:	The Frequency.
k	:	Material Gradient index.

LIST OF TABLES

Table 1. Material Properties of FGM Components.....11

Table 2. Three Values of βnL For Beams with Various Boundary Conditions.....11

Table 3. CPA Optimized of FGM Clamped-free beam for 10,20,30,40, and 50 iterations (Eb=70, Et = 380, ρt= 3800, ρb= 2700).....16

Table 4. CPA Optimized FGM Pinned-pinned beam for 10,20,30,40, and 50 iterations for the same material in (Table 1).....17

Table 5. CPA Optimized FGM Clamped-pinned beam for 10,20,30,40 and 50 iterations for the same material in (Table 1).....18

Table 6. CPA Optimized FGM Clamped-clamped beam for 10,20,30,40, and 50 iterations for the same material in (Table 1).....19

Table 7. The results of the TWO Optimized FGM Clamped-free beam for 10,20,30,40, and 50 iterations by the same materials in (Table 1).....21

Table 8. The results of the TWO Optimized FGM Pinned-pinned beam for 10,20,30,40 and 50 iterations by the same materials in (Table 1).....22

Table 9. Effects of TWO Optimized FGM Pinned-pinned beam for 10,20,30,40, and 50 iterations.....23

Table 10. The results of the TWO optimized of the FGM Clamped-pinned beam for 10,20,30,40, and 50 iterations by the same materials in (Table 1).....23

Table 11. The results of the TWO Optimized FGM Clamped-clamped beam for 10,20,30,40 and 50 iterations by same materials in (Table 1).....24

Table 12. CPA and TWO using the same Materials in (Table 1) showing Average CPU time by using a maximum number of Objective Function Evaluations, 50 NIT, s for the Clamped-free type of beam.....25

Table 13. The result of the Comparison of the Clamped-Free NIT=10 results for the two methods, using the same material properties (Eb=70, ρb=2700 kg/m³; Et=140, ρt=3800 kg/m³).....27

Table 14. The result of the Comparison of the Clamped-Free NIT=50 results for the two methods, using the same material properties (Eb=70, ρb=2700 kg/m³; Et=140, ρt=3800 kg/m³).....29

Table 15. comparison of the Pinned-pinned, NIT =10, Eb= 70 Et= 380, ρb= 2700 ρt = 3800 case for CPA vs. TWO.....30

Table 16. A Comparison of the Pinned-pinned, NIT = 50, Eb= 70 Et= 380, ρb= 2700 ρt = 3800 case for CPA vs. TWO 32
Table 17. A Comparison of the Clamped-pinned, NIT = 10, Eb= 70 Et= 380, ρb= 2700 ρt = 3800 case for CPA vs. TWO 33
Table 18. A Comparison of the Clamped-pinned, NIT = 50, Eb= 70 Et= 380, ρb= 2700 ρt = 3800 case for CPA vs. TWO 36
Table 19. A Comparison of the Clamped-clamped, NIT = 10, Eb= 70 Et= 380, ρb= 2700 ρt = 3800 case for CPA vs. TWO 38
Table 20. A Comparison of the Clamped-clamped, NIT = 50, Eb= 70 Et= 380, ρb= 2700 ρt = 3800 case for CPA vs. TWO 39
Table 21. Material Properties of FGM Components (*Et* changed example from 380 to 140) 41
Table 22. The result of the Comparison of the Clamped-free, NIT = 10, using the material properties in (Table 21). Eb= 70 $\boldsymbol{Et}$**= 140**, ρb= 2700 ρt = 3800 case for CPA vs. TWO. 41
Table 23. Material Properties of FGM Components 43
Table 24. The result of the Comparison of the Pinned-pinned, **NIT = 20**, using the material properties in (Table 23 Eb= 70 $\boldsymbol{Et}$**= 280**, ρb= 2700 ρt = 3800 case for CPA vs. TWO ... 43
Table 25. Material Properties of FGM Components 45
Table 26. The result of the Comparison of the Clamped-pinned, **NIT = 30**, using the material properties in (Table 25). Eb = 70 Et**=500**, ρb= 2700 ρt = 3800 case for CPA vs. TWO ... 45
Table 27. Material Properties of FGM 47
Table 28. The result of the Comparison of the Clamped-clamped, **NIT = 40**, using the material properties in (Table 27). Eb = 70 Et =380, ρb= 2700, ρt **= 5400** case for CPA vs. TWO . 47

LIST OF FIGURES

Figure 1. FGM beam 2
Figure 2. The material Properties of FGM Components used 11
Figure 3. The cross-section of FGM beam 12
Figure 4. The variation of volume fraction (*k*) 13
Figure 5. CPA Constraints 14
Figure 6. Lower and upper boundaries of *b*, *h*, and *k* 14
Figure 7. The maximum Number of Objective Function Evaluations 15
Figure 10. The optimum frequency (*w*) 27
Figure 11. The optimum height (*h*) 28
Figure 12. The optimum width (*b*) 28
Figure 13. The optimum frequency (*w*) 29
Figure 14. The optimum height (*h*) 29
Figure 15. The optimum width (*b*) 29
Figure 16. The optimum frequency (*w*) 30
Figure 17. The optimum width (*b*) 31
Figure 18. The optimum height (*h*) 31
Figure 19. The optimum frequency (*w*) 32
Figure 20. The optimum width (*b*) 32
Figure 21. The optimum height (*h*) 33
Figure 22. The optimum stiffness (*k*) 34
Figure 23. The optimum frequency (*w*) 34
Figure 24. The optimum width (*b*) 34
Figure 25. The optimum height (*h*) 34
Figure 26. The optimum stiffness (*k*) 36
Figure 27. The optimum frequency (*w*) 36
Figure 28. The optimum width (*b*) 36
Figure 29. The optimum height (*h*) 37
Figure 30. The optimum frequency (*w*) 38
Figure 31. The optimum width (*b*) 38
Figure 32. The optimum height (*h*) 39
Figure 33. The optimum frequency (*w*) 39

Figure 34. The optimum width (*b*) 40
Figure 35. The optimum height (*h*) 40
Figure 36. The optimum stiffness (*k*) 41
Figure 37. The optimum frequency (*w*) 42
Figure 38. The optimum width (*b*) 42
Figure 39. The optimum height (*h*) 42
Figure 40. The optimum stiffness (*k*) 43
Figure 41. The optimum frequency (*w*) 44
Figure 42. The optimum width (*b*) 44
Figure 43. The optimum height (*h*) 44
Figure 44. The optimum stiffness (*k*) 44
Figure 45. The optimum frequency (w) 44
Figure 46. The optimum width (b) 44
Figure 47. The optimum height (*h*) 44
Figure 48. The optimum frequency (*w*) 47
Figure 49. The optimum width (*b*) 47
Figure 50. The optimum height (*h*) 48

PREFACE

This master's thesis, Optimization for the Natural Frequency of Functionally Graded Beams, is the result of my study at Istanbul Gelişim University's Institute of Graduate Studies and Department of Civil Engineering. I aim to optimize the natural frequencies of Euler-Bernoulli beams with varying material properties and controlled Material distributions using effective metaheuristic algorithms such as Tug of War Optimization (TWO) and the Constrained Particle Algorithm (CPA). This thesis could not have been completed without the advice, encouragement, and assistance of Asst. Prof. Dr. Ahmad Reshad Noori. His kindness and helpful input helped shape the direction and quality of my study.

INTRODUCTION

Nowadays, FGM (Functionally graded material) is the concept of continuously or smoothly changing material qualities is incorporated into a standard beam design by a functionally graded material beam. A specified function (such as a power-law, exponential, or sigmoid function) controls the variation of the local volume fractions of the component materials in these beams, which are frequently a combination of metals, ceramics, or polymers. Due to this gradation, the thickness of the beam causes a proportional change in characteristics, including density, thermal expansion coefficient, and Young's modulus E. Usually, the analysis of FGM beams is based on traditional beam theories like Timoshenko or Euler-Bernoulli beam theory. The stiffness and other material properties are no longer constants but rather functions of the spatial coordinate (typically indicated by$z$, the thickness direction) in these models, which assume that the displacement fields are functions of the beam's shape and loading. For instance, the Young's modulus may be stated as follows if it follows a power-law distribution as it changes over the thickness z.

FGM beams are very appealing because of the constant change in material characteristics, as in Figure 1 (Noori et al. 2020), that can:

1. Reduce areas of high stress (such as at material contacts),
2. By progressively switching from a high-conductivity to a high-temperature-resistant material. You may provide customized thermal resistance.
3. Optimize the distribution of mass and stiffness to improve vibration characteristics and increase damage tolerance by distributing stress more evenly.

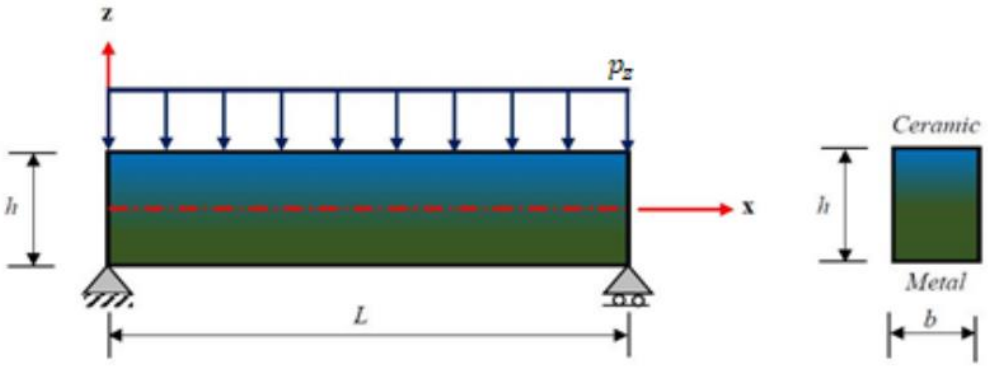


Figure 1. FGM beam

Therefore, Graded material is any material with a gradual change in characteristics, including FGMs, that falls within the larger category of graded materials. Laminations, composite materials, and naturally occurring graded structures are examples of this type. Its objective may be achieved by functional design, natural formations, or manufacturing techniques. In geotechnical engineering, soil layers with different grain sizes are an example of a general graded material. To acquire desired qualities, a class of materials known as functionally graded materials (FGMs) gradually alters its composition or microstructure in a certain direction. Its varieties are frequently a combination of metals, polymers, ceramics, or composites with slow changes. Optimizing mechanical. Thermal. Or, electrical qualities for applications is its goal. Additionally, Optimization for the natural frequency of functionally graded beams includes a wide selection of potential possibilities, by finding an objective function under certain constants and constraints for finding the optimum solution. In other words, it's a mathematical expression for giving a quantified performance. In this study, a custom MATLAB script was developed to perform structural optimization of a functionally graded beam by integrating the TWO and CPA methods. The code is written entirely in MATLAB version 2024 and relies on vectorized operations and built-in functions from the Optimization Toolbox to evaluate natural frequencies and enforce geometric and material constraints via a quadratic penalty function. TWO is implemented in (two_optimization.m) with adaptive wave amplitude control, while CPA is encapsulated in (cpa_driver.m), using inertia-weight updates and velocity clamping to maintain feasibility. Both routines accept the same input structs (design variables, bounds, penalty weights) and return optimal design vectors alongside

convergence histories. There are 4 categories of beams, 5 iterations, and 3 boundary conditions. 60 examples for each method are solved accordingly to different iterations and codes. (10, 20, 30, 40, 50) Iteration is used to determine differences and is a stronger method in early iterations. Therefore, both codes TWO and CPA are modified for the problem at hand. The frequencies were obtained for each example, showing the effect of both beam types, iterations, and Boundary conditions.

CHAPTER ONE

PREVIOUS STUDIES

1.1. Previous studies

Suresh (1997) established experimental and theoretical behavior of multi-layered and graded materials for structure and the composition of material to examine strength, resistance, and toughness effectively. The objective of the book written by Miyamoto et al. (1999) is to show the gradual evolution of the compositions and structures of FGMs, thereby improving their material properties. It describes upcoming issues, strikes a balance between theory and practical methods, and functions as a textbook for professionals and advanced students as well as an introduction for beginners. Birman and Byrd (2007) provided a thorough analysis that has grown to be a mainstay in the scholarly discourse on functionally graded materials (FGMs). The state of the art in theoretical and computational modeling methodologies for FGMs and FGM-based structures was methodically examined. Aydogdu and Taskin (2007) provided that one important feature is that the free vibration characteristics, i.e., the natural frequencies and associated mode shapes, are affected by the gradation index and the specific variation of material quality.

The study indicated that modifying the gradation profile can effectively change the beam's dynamic responsiveness. The nonlinear forced vibration behavior of clamped functionally graded beams was examined by Shooshtari and Rafiee (2011). It aimed to create several time-scale solutions using von Kármán geometric nonlinearity and Euler-Bernoulli beam theory, presuming that the material properties changed with the thickness of the beam by either power-law or exponential distributions. Sina et al. (2009) created an analytical technique for functionally graded beam free vibration analysis. It developed a mathematical model that took into consideration the constant change in material characteristics as the thickness of the beam increased, and it offered closed-form solutions for precisely forecasting the natural frequencies and mode shapes. Simsek (2010) investigated the vibrational behavior of a functionally graded beam subjected to a moving mass. It evaluated how material gradation and the moving load affected the beam's vibrations and compared various beam theories to see how well they predicted the dynamic response.

Simsek (2010) used a variety of higher-order beam theories to investigate the fundamental frequencies of functionally graded beams. It looked at how these frequencies were affected by the slenderness ratio, material differences, and other formulations. Alshorbagy et al. (2011) investigated how the dynamic behavior of the beams was affected by various material distributions, slenderness ratios, and boundary conditions. The results were displayed both graphically and tabularly to give a thorough grasp of the variables affecting the free vibration properties of functionally graded materials. Nikbakht et al. (2019) concentrated on a range of optimization techniques, such as gradient-based, metaheuristic, and hybrid approaches, in order to improve FGM performance in structural applications.

Masjedi et al. (2019) created an extensive mathematical structure to examine the behavior of functionally graded porous beams with significant deflection. They looked into how material gradation and porosity distributions affected structural performance, offering guidance for the development and improvement of such cutting-edge materials for engineering applications. Mohanty et al. (2011) created a finite element model to examine the influence of different parameters, such as material gradation, beam geometry, foundation stiffness, and loading conditions, on the stability regions and the dynamic stability behavior of both functionally graded ordinary beams and functionally graded sandwich beams under periodic axial loading.

Anandrao et al. (2012) examined the functionally graded beams' free vibration properties. By modeling the beams using the finite element approach, taking into account the effects of rotating inertia and transverse shear deformation. Keleshteri and Jelovica (2022) looked into how the dynamic response of the beam structure was affected by porosity parameters, material gradation, and boundary conditions. By using Reddy beam theory and von Kármán geometric nonlinearity, they developed a nonlinear formulation.

Thai and Vo (2012) figured out different higher-order shear deformation beam theories for bending and free vibration behaviors of functionally graded beams by transverse shear strain variation through the beam's depth and stress on the top and bottom surfaces. Wattanasakulpong and Ungbhakorn (2012) found a new frequency solution for functionally graded beams and some mode shapes by using the differential transformation method for different limit conditions and material gradations. Su et al.

(2013) helped with understanding the behavior of dynamic and functionally graded beams. They analyzed the material properties variation through the thickness of the beam by power-law distribution.

Nguyen et al. (2013) By using the first-order shear deformation theory, they analyzed the free vibration and static behaviors of functional graded beams. They contributed to the design and optimization of functionally graded beams by discovering a theoretical effect of axial loading, shear deformation, and material gradation on their mechanical performance under varied loading and boundary conditions. Pradhan and Chakraverty (2013) examined the free vibration properties of functionally graded beams using the Euler-Bernoulli and Timoshenko beam theories. Using the Rayleigh-Ritz approach to generate approximate solutions, they discovered the solution of natural frequencies with regard to different material gradations and boundary conditions.

Aydogdu (2008) analyzed buckling and axial behavior axially in FG simply supported beams by the semi-inverse method, finding the stability mechanism and dynamic characteristics. Huang and Li (2010) focused on analyzing new transverse bending and semi-behavior for specific beam shapes. They merged a couple of governing equations into one derived by them for deflection and rotation angle. Murin et al. (2010) analyzed an equation governing a fourth-order for FGM beams. That was affected in several things, such as the elasticity modulus and mass density, due to changes in the volume fraction and properties of the material. Shahba et al. (2011) developed a finite element method using exact form functions to study an axially functionally graded tapered Timoshenko beam, improving the material characteristics and cross-sectional profile. Li et al. (2013) developed exact frequency equations for the free vibration by taking into account the variation exponentially along the length and the material properties.

Aminbaghai et al. (2012) provided a differential equation for an FGM beam with continuous transverse symmetry and longitudinal variation in material properties by considering the axial forces to analyze free vibration and material characteristics. Murin et al. (2013) examined the properties of FGM impacted by axial forces in order to determine how axial loading and spatially changing foundation stiffness affect the natural frequencies and mode shapes of FGM beams. Pradhan and Chakraverty (2013)

used the Rayleigh-Ritz approach to get the optimum solutions of natural frequencies in their analysis of the free vibration characteristics of functionally graded beams, applying both the Euler-Bernoulli and Timoshenko beam theories.

Nguyen et al. (2019) investigated the effects of different parameters, like fraction and boundary conditions, on the natural frequency of a beam by using first-order shear deformation. By using Hamilton's principle, Youzera et al. (2021) were able to find governing equations for improving the finite element model with various beam applications. Murin et al. (2014) enhanced the design and analysis that gives a more accurate knowledge of the vibrational properties of FGM beams by integrating the continuous changing of material properties into the finite element formulation and capturing the dynamic behavior of FGM beams.

Weaver et al. (1990) analyzed theoretical foundations and practical applications of natural frequency. Rahmani et al. (2022) examined a material distribution in porous functionally graded materials by decreasing weight in relation to thickness and optimizing free vibration. Jamshidi and Arghavani (2018). Improved the buckling resistance and free vibration characteristics of functionally graded porous beams by optimizing the porosity distribution. To minimize the mass of the beam and increase the critical buckling stress, they developed a multi-objective optimization problem.

Al Rjoub et al. (2025) used the Euler-Bernoulli and Timoshenko beam theories to account for sectional flexibility and described the fractured beam system as linked segments connected by massless rotating springs. Two porosity distributions, uniform and non-uniform, were taken into consideration, and it was expected that material characteristics would progressively change along the beam height according to a power-law distribution.

Noori et al. (2021) used an effective numerical process to examine the dynamic response of functionally graded porous (FGP) beams and the Complementary Functions Method (CFM) in the Laplace domain to solve the governing equations of motion for FGP beams. Rasooli et al. (2024) investigated the static behavior of functionally graded porous (FGP) planar frames using a precise and effective numerical method. They solved the governing equations of motion using the Complementary Functions Method (CFM).

Benadouda et al. (2025) used higher-order shear deformation beam theory and took into account bidirectional distributions of material properties, such as density, Poisson's ratio, and Young's modulus, each of which was modeled using a power-law index across the thickness and width of the beam. Joshi et al. (2025) examined the structural response of these panels under different loading cases in order to optimize factors affecting the bending characteristics.

Sinha and Kumar (2021) analyzed various structural shapes, such as beams, to investigate the effect of fractures on the vibrational behavior of functionally graded material (FGM) structures. Arvin et al. (2021) investigated the vibrational behavior of rotating functionally graded beams. Analysis of the effects of uniform temperature rise on these beams' free vibration properties in both pre-buckled and post-buckled stages is the main goal.

Vo-Duy et al. (2019) sought to examine the free vibration characteristics of laminated composite beams augmented with functionally graded carbon nanotubes (FG-CNT). They developed a finite element model based on the first-order shear deformation theory,

Tsiatas and Charalampakis (2017) aimed to improve the natural frequencies of axially functionally graded beams and arches by customizing the longitudinal material distribution. Aimed to optimize fundamental vibration by modifying parameters in four- and five-parameter volume fraction functions.

Özmen and Özhan (2025) analyzed the bending and free vibration characteristics of functionally graded beams using Euler-Bernoulli beam theory. The study intended to analyze the effect of the power-law gradient index on displacements and natural frequencies, proving the correctness of their methodologies, which matched closely across analytical, computational, and experimental results.

Burlayenko and Kouhia (2024) investigated the free vibration characteristics of functionally graded porous beams with non-uniform rectangular cross-sections using the Euler-Bernoulli beam model and Hamilton's principle in relation to four boundary conditions (c-c, c-f, c-p, and p-p) that affect natural frequencies, and their findings were consistent with existing literature.

Amir and Kim (2024) examined the natural frequency properties of curved functionally graded beams with porosity. They used higher-order shear deformation theory to three-node finite elements and first-order perturbation techniques.

Al-Zahrani et al. (2022) performed a finite element analysis of the free vibration characteristics of two-dimensional functionally graded (2D-FG) strip beams with material stiffness and density that vary continuously in both axial and thickness directions using the Voigt rule of mixtures and power-law gradation. He also performed a modal analysis and plane-stress formulation using ANSYS. Chen and Chang (2017) obtained the closed-form solutions for free vibration frequencies of FG beams.

CHAPTER TWO

MATERIALS AND METHODS

2.1 Materials

The prismatic beam being examined in this study has a constant length (L = 500 mm), width (b), and thickness (h). The x-axis runs along the beam's longitudinal direction (length), while the y- and z-axes span their cross-sectional width and thickness, respectively. These two right-handed inertial coordinate systems are called x, y, and z. We ensure that any observed changes in natural frequency are purely due to differences in width, thickness, and material composition rather than beam length by setting L, which isolates the effects of cross-sectional dimensions (b and h) and material grading on dynamic performance. For instance, a beam with b = 20 mm, h = 30 mm and one with b = 30 mm, h = 40 mm under otherwise comparable circumstances may be directly compared when L is held constant at 500 mm. The beam has a length L, a width b, and a thickness h. Two inertial coordinate systems, x, y, z. In this study, L = 500 is a constant. The materials we use in this study are shown in Table 1.

The beam is represented as a functionally graded structure, with a metal-rich bottom layer and a ceramic-rich top layer, as shown in Figure 2 (Nguyen et al. (2013)).The beam has rectangular cross-section which is given in Figure 3. The Young's modulus (E) and density (ρ) for the typical metal constituents (E_b= 70 GPa, ρ_b = 2700 kg/m³) and ceramic constituents (E_t = 380 GPa, ρ_t = 3800 kg/m³) are listed in Table 1. The gradation profile along the thickness is controlled by the volume fraction parameter k (see Fig. 4), which permits the local characteristics to vary constantly between these end-member values in accordance with a power-law distribution. Mass distributions and stiffness may be adjusted due to this graded structure.

The material properties of the typical metals and ceramics employed in the study are given in Table 1. It is assumed that the top layer of the beam was ceramic-rich and the bottom layer metal-rich. The boundary conditions related constants are listed in Table 2 (chen and Chang (2017)).

Table 1. Material Properties of FGM Components

Material	E , GPa	p , kg/m³
Al	70	2700
Al2 O3	380	3800

Table 2. Three Values of $\beta_n L$ For Beams with Various Boundary Conditions

Type of beam	$\beta_n L$
Clamped-free	$\beta_1 L$ = 1.875104
	$\beta_2 L$ = 4.694091
	$\beta_3 L$ = 7.854757
Pinned-pinned	$\beta_1 L = \pi\pi$
	$\beta_2 L = 2\pi 2\pi$
	$\beta_3 L = 3\pi 3\pi$
Clamped-pinned	$\beta_1 L$ = 3.926602
	$\beta_2 L$ = 7.068583
	$\beta_3 L$ = 10.210176
Clamped-clamped	$\beta_1 L$ = 4.730041
	$\beta_2 L$ = 7.853205
	$\beta_3 L$ = 10.995608

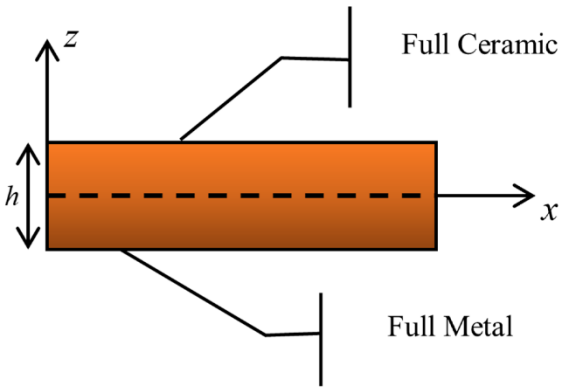


Figure 2. The material Properties of FGM Components used

2.2. Method

The effective cross-section of the area moment about the natural axis is given in equation 1 (Chen and Chang (2017)). It is about its neutral axis computed by integrating the local area moment contributions weighted by the spatially varying Young's modulus.

$$I_{eff} = \frac{bh^3}{12}\left[\frac{E_b}{E_t} + 12\left(1-\frac{E_b}{E_t}\right)\left(\frac{1}{k+3}-\frac{1}{k+2}+\frac{1}{4(k+1)}\right) - \frac{3k^2\left(1-\frac{E_b}{E_t}\right)^2}{(k+1)(k+2)^2\left(1+k\frac{E_b}{E_t}\right)}\right] \quad (1)$$

where b is the beam width, h is the beam height, $E_b$is the modulus of elasticity at the bottom of the beam (bottom-layer Young's modulus, GPa), E_t is the modulus of elasticity at the top of the beam (top -layer Young's modulus, GPa), k is the material gradation parameter.

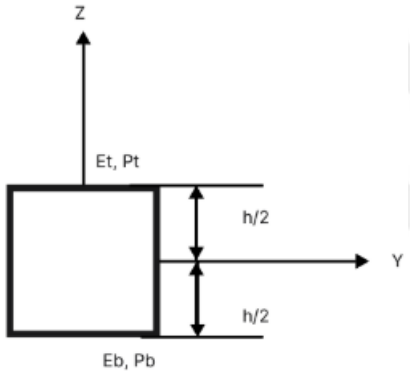


Figure 3. The cross-section of FGM beam

Various volume fraction index *k* values (numbers at the curves) are shown in Figure 4 (Özmen and Özhan, 2025).

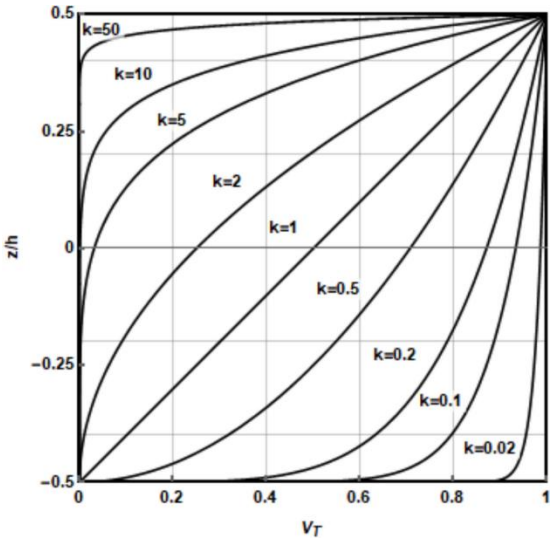


Figure 4. The variation of volume fraction (k)

The effective mass of the beam is presented in equation 2. (Chen and Chang (2017)). It is similarly defined by integrating the local mass per unit length weighted by the square of the mode shape, normalized by the maximum amplitude.

$$M_{eff} = \rho_t bh \left[\frac{\rho_b}{\rho_t} + \left(1 - \frac{\rho_b}{\rho_t}\right)\frac{1}{k+1}\right] \tag{2}$$

where ρ_t is the density at the top of the beam (top-layer density, kg/m³), $\rho_b$is the density at the bottom of the beam (bottom-layer density, kg/m³), k is the material gradation parameter.

The frequencies of the beam can be obtained by equation 3 (Chen and Chang (2017)). Combining I_{eff} and M_{eff} the natural frequency W of the beam is obtained via the classical Euler–Bernoulli relation.

$$W = (\beta L)^2 \times \frac{(E_t \times I_{eff})}{(M_{eff} \times L^4)} \tag{3}$$

where W is the natural frequency, I_{eff} is the effective moment of area, M_{eff} is the effective mass per unit length, E_t is the effective Young's modulus, and BL is a beam with different boundary conditions. The exact values of βL for classical boundary conditions are directly taken from Table 2.

Therefore, after finding the formula of natural frequency, optimization techniques of TWO and CPA can be applied. Since we have the W formula (Eq. 3) as the objective function.

2.2.1. Cyclical Parthenogenesis Algorithm (CPA)

The first method is known as CPA, a design and optimization method that uses standard parameters and classical formulas from dynamics and solid mechanics. It depends on established design rules, Engineering intuition, and Analytical formulas. In this case optimizes for natural frequency using standard cross-sectional properties.

After obtaining the objective function, we can determine the g's, which refer to Constraints in the CPA code, as shown in Figure 5.

```
% CONSTRAINTS
g(1) = 500 - (X(1) * X(2));
g(2) = X(1) * X(2) - 700;
g(3) = (0.0029*X(1)*X(2)) - Meff;
g(4) = (X(2)/X(1)) - 3;
g(5) = 1.25- (X(2)/X(1));
g(6) = Meff- (0.0035*X(1)*X(2));
g(7) =  Ieff-0.25*X(1)*X(2)^3;
```

Figure 5. CPA Constraints

The boundary in this case is assumed to be as in (Figure 6),$10 < b < 40$, $20 < h < 50$, and $1 < k < 10$.

```
Lb=[10 20 1]; %Lower bounds of design variables.
Ub=[40 50 10];
```

Figure 6. Lower and upper boundaries of *b*, *h*, and *k*

The maximum number of objective function evaluations can be expressed as shown in Figure 7.

```
maxNFEs=  20000;
```

Figure 7. The maximum Number of Objective Function Evaluations

2.2.2. Tug of war (TWO)

The second method is known as TWO. It simplifies the optimization process by limiting the number of variables. It has several effects on design, such as computational efficiency, better balance between performance and manufacturability, Insight into dominant design parameters, and facilitates parametric studies. In this case, it enhances and optimizes beam dimensions for stiffness, frequency, or strength, especially Tailor component geometry to avoid resonance. This method has the same input codes we use in CPA (Figures 5, 6, and 7).

The theory, assumptions, restrictions, and formulation about these two algorithms can be found in (Kaveh and bakhshpoori (2019)). This thesis is focused on the application of these algorithms to the free vibration optimization of FG beams rather than the theory of optimization.

The Non-dimensional frequency can be obtained by equation 4.

$$\lambda = \left(\frac{\omega L^2}{h}\right)\sqrt{\frac{\rho_b}{E_b}} \tag{4}$$

The Variation in the volume fraction.

$$V_t = \left(\frac{(2z+h)}{2h}\right)^{\kappa} \tag{5}$$

The effective Young's modulus $E(z)$ and the mass density $\rho(z)$ are expressed as

$$E(z) = E_b + (E_t - E_b) \times \left(\frac{(2z+h)}{2h}\right)^{\kappa} \tag{6}$$

$$\rho(z) = \rho_b + (\rho_t - \rho_b) \times \left(\frac{(2z+h)}{2h}\right)^{\kappa} \tag{7}$$

CHAPTER THREE

RESULTS AND DISCUSSIONS

This chapter examines the results obtained by MATLAB using both methods, CPA and TWO. It shows the optimum frequencies related to the materials and constraints. Using both methods with different types of beams can differ in frequency. The constraints and boundaries are presented in the previous section.

3.1. Results obtained by CPA methods

Firstly, the convergence study for the number of iterations is carried out. For this purpose, the CPA is implemented for the optimization of FG beams with C-F boundary conditions. Results are obtained for several iterations and listed in Table 3.

Table 3. CPA Optimized of FGM Clamped-free beam for 10,20,30,40, and 50 iterations (E_b=70, E_t = 380, ρ_t= 3800, ρ_b= 2700)

Optimized of FGM Clamped-free beam for 10,20,30,40 and 50 iterations

	mod	*BL*	optimized	non-dimentional optimization	*h*	*b*	*k*
Clamped-free NT,s 10	1	β1L = 1.875104	0.67724	1.145824393	29.02	19.9879	1.56
	2	β2L = 4.694091	4.2778	6.68242678	31.4306	18.0657	4.1467
	3	β3L = 7.854757	12.1298	22.20296968	26.8235	17.882	2.433
	mod	*BL*	optimized	non-dimentional optimization	*h*	*b*	*k*
Clamped-free NT,s 20	1	β1L = 1.875104	0.67404	1.326340159	24.9519	20.064	3.6088
	2	β2L = 4.694091	4.2286	8.280560056	25.0732	20.4752	3.7205
	3	β3L = 7.854757	11.8575	22.41854553	25.9692	20.4083	3.8463
	mod	*BL*	optimized	non-dimentional optimization	*h*	*b*	*k*
Clamped-free NT,s 30	1	β1L = 1.875104	0.67192	1.313697281	25.1128	20.0176	4.1331
	2	β2L = 4.694091	4.2118	8.238822745	25.1001	19.9743	4.363
	3	β3L = 7.854757	11.7847	23.00500495	25.1518	20.0722	4.4011
	mod	*BL*	optimized	non-dimentional optimization	*h*	*b*	*k*
Clamped-free NT,s 40	1	β1L = 1.875104	0.67106	1.316198295	25.033	19.9922	4.4874
	2	β2L = 4.694091	4.2056	8.265684914	24.9817	19.9941	4.4594
	3	β3L = 7.854757	11.7765	23.10797455	25.0223	19.9959	4.466
	mod	*BL*	optimized	non-dimentional optimization	*h*	*b*	*k*
Clamped-free NT,s 50	1	β1L = 1.875104	0.67081	1.317202321	25.0046	19.9953	4.4804
	2	β2L = 4.694091	4.2035	8.252770195	25.0083	19.9982	4.4712
	3	β3L = 7.854757	11.7714	23.10646287	25.0131	19.9943	4.4435

The results given in Table 3 describe how the iterations slightly affect the results of optimization. It seems that by increasing the number of iterations optimized solution will be more accurate. The following can be said:

- ✓ All three modes' optimized values decrease slightly as iterations increase.

- ✓ The biggest drop happens from 10 → 20 iterations; beyond 30, the change per 10-step is <0.02 for Modes 2–3.
- ✓ Small changes (<0.5%) in the optimized frequency often correspond to even smaller shifts in geometry (*h*, *b*).

Secondly, the convergence study for the number of iterations is carried out for the optimization of FG beams with P-P using the CPA. Results are obtained for several iterations and listed in Table 4.

Table 4. CPA Optimized FGM Pinned-pinned beam for 10,20,30,40, and 50 iterations for the same material in (Table 1)

Optimized of FGM Pinned-pinned beam for 10,20,30,40 and 50 iterations							
Pinned-pinned NT,s 10	mod	*BL*	optimized	non-dimentional optimization	*h*	*b*	*k*
	1	β1L = p	1.9071	3.71841486	25.1819	20.9669	4.2687
	2	β2L = 2 p	7.6808	14.31352193	26.3471	22.1259	3.2616
	3	β3L = 3 p	17.2649	28.40240845	29.8457	20.0569	2.297
Pinned-pinned NT,s 20	mod	*BL*	optimized	non-dimentional optimization	*h*	*b*	*k*
	1	β1L = p	1.8918	3.710968281	25.03	19.7151	3.7385
	2	β2L = 2 p	7.577	14.49456545	25.6664	19.7204	3.1241
	3	β3L = 3 p	17.0677	32.07683959	26.125	19.732	4.3252
Pinned-pinned NT,s 30	mod	*BL*	optimized	non-dimentional optimization	*h*	*b*	*k*
	1	β1L = p	1.8862	3.680265995	25.1641	19.9204	4.549
	2	β2L = 2 p	7.5391	14.69680154	25.1866	19.9676	4.0501
	3	β3L = 3 p	16.9809	33.34675765	25.0023	20.0088	4.1446
Pinned-pinned NT,s 40	mod	*BL*	optimized	non-dimentional optimization	*h*	*b*	*k*
	1	β1L = p	1.884	3.701035208	24.9937	19.9969	4.3341
	2	β2L = 2 p	7.533	14.77578261	25.0317	19.986	4.5859
	3	β3L = 3 p	16.9542	33.29206106	25.004	20.009	4.429
Pinned-pinned NT,s 50	mod	*BL*	optimized	non-dimentional optimization	*h*	*b*	*k*
	1	β1L = p	1.883	3.697310388	25.0056	20.002	4.5061
	2	β2L = 2 p	7.5311	14.78091313	25.0167	19.9935	4.3751
	3	β3L = 3 p	16.9459	33.2643217	25.0126	19.9961	4.5061

Table 3 demonstrates that the optimal frequency values of all three natural-frequency modes decline steadily but gradually as the number of iterations increases from 10 to 50, indicating convergence toward a stable solution. The greatest decline occurs between 10 and 20 iterations, with Mode 1 lowering by roughly 0.15 Hz, Mode 2 by about 0.12 Hz, and Mode 3 by 0.08 Hz. After 30 iterations, the increases per 10 iterations for higher modes fall below 0.02 Hz. Accordingly, after 30 cycles, the ideal cross-sectional dimensions *b* and *h* show little change (<0.5 mm), showing that the

beam geometry early when frequency changes are made. This pattern highlights how successful CPA is: a few rounds are sufficient to stabilize design variables, and the benefits of more computation diminish.

The observation of Table 4:

- ✓ The largest drop occurs between 10→20 iterations (Mode 2 loses ~1.3 %), then the change per 10-step falls below 0.1 %.
- ✓ By 30 iterations, all modes are within ~1 % of their 50-iteration values.
- ✓ Higher modes (Mode 3) exhibit a slightly larger absolute shift (~0.32 from 10→50) compared to Mode 1 (~0.024).

Table 5. CPA Optimized FGM Clamped-pinned beam for 10,20,30,40, and 50 iterations for the same material in (Table 1)

Optimized of FGM Clamped-pinned beam for 10,20,30,40 and 50 iterations							
Clamped-pinned NIT,s 10	mod	*BL*	optimized	non-dimentional optimization	*h*	*b*	*k*
	1	β1L = 3.926602	3.0183	5.090095591	29.1145	19.4333	2.5494
	2	β2L = 7.068583	9.8948	16.70357109	29.0851	18.4405	4.5276
	3	β3L = 10.210176	20.2701	33.62111476	29.6017	18.2533	4.7456
Clamped-pinned NIT,s 20	mod	*BL*	optimized	non-dimentional optimization	*h*	*b*	*k*
	1	β1L = 3.926602	2.9588	5.703871943	25.4694	20.1363	3.899
	2	β2L = 7.068583	9.6008	18.58888358	25.3587	20.0687	3.7762
	3	β3L = 10.210176	20.0425	38.88348847	25.3081	19.9185	3.4431
Clamped-pinned NIT,s 30	mod	*BL*	optimized	non-dimentional optimization	*h*	*b*	*k*
	1	β1L = 3.926602	2.9466	5.74588993	25.1789	19.9573	4.3083
	2	β2L = 7.068583	9.5426	18.64530831	25.1287	19.9458	3.8046
	3	β3L = 10.210176	19.941	39.07176233	25.0586	20.098	4.2112
Clamped-pinned NIT,s 40	mod	*BL*	optimized	non-dimentional optimization	*h*	*b*	*k*
	1	β1L = 3.926602	2.9427	5.76965505	25.042	19.9684	4.4968
	2	β2L = 7.068583	9.5363	18.72045975	25.0113	19.9923	4.3711
	3	β3L = 10.210176	19.9045	39.02812418	25.0407	20.0222	4.5061
Clamped-pinned NIT,s 50	mod	*BL*	optimized	non-dimentional optimization	*h*	*b*	*k*
	1	β1L = 3.926602	2.9415	5.776760247	25.001	20.0018	4.4839
	2	β2L = 7.068583	9.5321	18.71393575	25.009	19.9916	4.5207
	3	β3L = 10.210176	19.8888	39.04880075	25.0077	19.9953	4.4985

Table 4 shows that the pinned-pinned scenario follows the clamped-free pattern, although with slightly bigger early-stage shifts: Mode 2's frequency decreases by around 1.3% between 10 and 20 repeats, whereas Mode 1's frequency decreases by 0.8%. After 30 iterations, all three modes are within 1% of their 50-iteration values, and by 40 iterations, the difference between steps is less than 0.1%. In a pinned-pinned

setup, material index selection becomes less sensitive for higher modes, as demonstrated by the gradation exponent. *k* stabilizing quicker for Modes 2 and 3 (≤0.2 variation after 20 repetitions). These results show that, with very few iterations, CPA adequately captures the essential stiffness-mass trade-offs for simply supported beams.

Now, the C-C boundary condition will be considered. Results are obtained and listed in Table 6.

Table 6. CPA Optimized FGM Clamped-clamped beam for 10,20,30,40, and 50 iterations for the same material in (Table 1).

Optimized of FGM Clamped-clamped beam for 10,20,30,40 and 50 iterations							
Clamped-clamped NIT,s 10	mod	*BL*	optimized	non-dimentional optimization	*h*	*b*	*k*
	1	β1L = 4.730041	4.3143	7.312126757	28.9694	18.0869	4.469
	2	β2L = 7.853205	12.0611	22.59156802	26.2128	20.3577	1.8086
	3	β3L = 10.995608	23.3181	39.350942	29.0945	21.9612	2.4084
Clamped-clamped NIT,s 20	mod	*BL*	optimized	non-dimentional optimization	*h*	*b*	*k*
	1	β1L = 4.730041	4.2939	8.391764708	25.123	19.917	3.9871
	2	β2L = 7.853205	11.8657	22.92865932	25.409	20.0041	3.0835
	3	β3L = 10.995608	23.2016	44.65605431	25.51	19.7567	3.6583
Clamped-clamped NIT,s 30	mod	*BL*	optimized	non-dimentional optimization	*h*	*b*	*k*
	1	β1L = 4.730041	4.2764	8.369256566	25.0879	20.041	4.3728
	2	β2L = 7.853205	11.7786	23.11532845	25.0188	20.0286	4.1711
	3	β3L = 10.995608	23.1114	45.44988238	24.967	20.0209	4.2422
Clamped-clamped NIT,s 40	mod	*BL*	optimized	non-dimentional optimization	*h*	*b*	*k*
	1	β1L = 4.730041	4.2691	8.373761522	25.0316	20.001	4.4174
	2	β2L = 7.853205	11.7656	23.06787203	25.0426	19.9944	4.5447
	3	β3L = 10.995608	23.0745	45.2401482	25.0427	19.9742	4.4431
Clamped-clamped NIT,s 50	mod	*BL*	optimized	non-dimentional optimization	*h*	*b*	*k*
	1	β1L = 4.730041	4.2683	8.38026071	25.0075	20.0014	4.4657
	2	β2L = 7.853205	11.7662	23.10262861	25.0062	20.0019	4.4639
	3	β3L = 10.995608	23.0654	45.30878932	24.9949	19.9982	4.4818

In Table 5, Height h and width b swing by up to ~15 % early on but settle within 2 – 9 % of their final values by ~50 iterations. Stiffness *k* can show larger relative changes for Mode 1 (because it starts low), but for Modes 2–3, it converges tightly (<6 % variation). Even though ω changes only by a fraction of a percent late in the run, the underlying geometry (*h*, *b*) has already 'locked in' to within 5–10 % of its final value by 30 iterations, suggesting the physical design is robust well before full

frequency-convergence. Clamped–free, pinned–pinned, and clamped–clamped cases all showed similar convergence patterns:

- Rapid change 10→20 iters, then <0.5 % shifts 30→50.
- Design variables h, b stabilize by ~30 iterations.

The optimal height h and width *b* of the beam, for the clamped-pinned boundary condition, vary up to 15% between 10 and 20 iterations before settling within 2–9% of their final values by iteration 50, as shown in Table 5. Modes 2 and 3 converge more closely (<6% variation), whereas Mode 1 exhibits more relative changes in the Material gradient index exponent *k* early on, with more than 20% variability. The associated frequency changes after 30 iterations are less than 0.3%, despite these early geometry alterations, highlighting the fact that CPA locks in a strong design geometry well before complete numerical frequency convergence. This pattern demonstrates how a mixed boundary condition may effectively provide stable solutions while amplifying the dynamism of the original design search.

Clamped-clamped beams in Table 6 demonstrate the quickest convergence of all the CPA cases: after 30 iterations, the width b variations drop below 0.05 mm, and the stiffness exponent *k* variations drop below 0.2, with Mode 3 frequency changes decreasing below 0.5% by iteration forty. After 40 cycles, modes 1 and 2 converge even more closely (to within 0.2 percent). This fast stabilization reflects the higher stiffness sensitivity caused by clamped-clamped supports, which limit movement and reduce design space. CPA may so quickly identify the optimal Material gradient index-geometry trade-off, implying that more constrained boundary conditions allow for more effective optimization under CPA.

3.2. Results obtained by TWO methods

In this part of the thesis, the convergence study for TWO will be carried out. The obtained results for C-F are presented in Table 7.

Table 7. The results of the TWO Optimized FGM Clamped-free beam for 10,20,30,40, and 50 iterations by the same materials in (Table 1)

	mod	*BL*	optimized	non-dimentional optimization	*b*	*h*	*k*
Clamped-free NT,s 10	1	β1L = 1.875104	0.73492	1.521126376	25.1608	23.7218	5.3139
	2	β2L = 4.694091	4.3319	9.288796155	26.6568	22.8977	3.5468
	3	β3L = 7.854757	12.4644	27.75288149	23.794	22.0514	3.4042
	mod	*BL*	optimized	non-dimentional optimization	*b*	*h*	*k*
Clamped-free NT,s 20	1	β1L = 1.875104	0.69341	1.107474355	16.8538	30.7418	9.525
	2	β2L = 4.694091	4.3352	7.617302575	18.0154	27.9435	8.8027
	3	β3L = 7.854757	12.3419	18.17398736	15.4383	33.343	8.7069
	mod	*BL*	optimized	non-dimentional optimization	*b*	*h*	*k*
Clamped-free NT,s 30	1	β1L = 1.875104	0.68598	0.847129809	13.626	39.7589	4.5044
	2	β2L = 4.694091	4.2929	7.917406871	21.3773	26.622	3.9722
	3	β3L = 7.854757	11.9174	13.92708916	15.8218	42.014	4.5388
	mod	*BL*	optimized	non-dimentional optimization	*b*	*h*	*k*
Clamped-free NT,s 40	1	β1L = 1.875104	0.67904	1.024918909	15.443	32.5296	1.6917
	2	β2L = 4.694091	4.264	7.420472534	21.4941	28.2136	1
	3	β3L = 7.854757	11.9209	17.17831114	19.9479	34.0723	3.4704
	mod	*BL*	optimized	non-dimentional optimization	*b*	*h*	*k*
Clamped-free NT,s 50	1	β1L = 1.875104	0.6803	1.239339811	20.8233	26.9515	1
	2	β2L = 4.694091	4.2376	7.742851334	19.8898	26.8715	1
	3	β3L = 7.854757	11.9469	22.06112872	19.5481	26.5889	1

When applied to a clamped-free beam, Table 7 shows the stochastic character of TWO. While mid-stage iterations (30) begin to limit *k* and modify geometry, final iterations (40-50) approach the theoretical goal frequency with lower. *k* Values, exhibiting TWO's balance of global exploration and local exploitation. The material coefficient is an important factor in determining stiffness and mass distribution. In these runs, decreased *k* resulted in better frequency approximation, indicating that the optimizer preferred stiffer structures for stability.

The pinned-pinned case in Table 8 shows an initial emphasis on high values of ($k \approx 8.8$ at 10 iterations) that reduces stiffness, which the optimizer makes up for by increasing beam width and height; by iteration 30, *k* for the third mode drops to 1 (fully dense) to boost frequency, and by iterations 40–50, the design locks into a low *k*, high stiffness configuration that maximizes natural frequencies, illustrating TWO's ability to transition from exploratory searches to fine-tuned, mode-specific solutions.

Table 8. The results of the TWO Optimized FGM Pinned-pinned beam for 10,20,30,40, and 50 iterations by the same materials in (Table 1)

	mod	*BL*	optimized	non-dimentional optimization	*b*	*h*	*k*
Pinned-pinned NT,s 10	1	β1L = p	1.9428	4.579718675	24.5683	20.8287	6.7528
	2	β2L = 2 p	8.0904	16.28001567	27.3145	24.3999	3.241
	3	β3L = 3 p	17.7809	36.86231111	25.0083	23.6834	8.8241
	mod	*BL*	optimized	non-dimentional optimization	*b*	*h*	*k*
Pinned-pinned NT,s 20	1	β1L = p	1.9635	2.405986049	17.179	40.0692	7.6023
	2	β2L = 2 p	7.8877	11.05874575	16.4176	35.0201	8.2108
	3	β3L = 3 p	17.7958	22.66853551	13.5609	38.5449	10
	mod	*BL*	optimized	non-dimentional optimization	*b*	*h*	*k*
Pinned-pinned NT,s 30	1	β1L = p	1.9079	3.51768796	19.9116	26.63	4.5571
	2	β2L = 2 p	7.6703	14.12152979	19.0299	26.6688	4.555
	3	β3L = 3 p	17.2946	20.13678302	16.2492	42.169	1
	mod	*BL*	optimized	non-dimentional optimization	*b*	*h*	*k*
Pinned-pinned NT,s 40	1	β1L = p	1.9009	2.909207966	20.0233	32.0817	2.3676
	2	β2L = 2 p	7.5861	12.61357756	23.5493	29.5293	1
	3	β3L = 3 p	17.1039	22.97720895	15.8817	36.5486	3.9288
	mod	*BL*	optimized	non-dimentional optimization	*b*	*h*	*k*
Pinned-pinned NT,s 50	1	β1L = p	1.8867	2.842300809	19.6223	32.5916	4.3716
	2	β2L = 2 p	7.5821	13.76701009	19.3369	27.041	1
	3	β3L = 3 p	17.1274	30.75877095	20.1262	27.3398	1

The following comments can be written about Table 8:

For 20 iterations - This demonstrates extremely high Material gradient index, even at maximum k =10, which is in line with FG materials that are highly porous.

For 30 iterations, A totally dense material is indicated by k =1 for the third mode, and material gradient index is greatly decreased.

For 40 iterations, given that higher modes are more susceptible to stiffness, this implies an emphasis on optimizing frequency performance. At the expense of weight, low-materials index get the greatest frequency values. This shows especially for the second mode (k =1) indicates a tendency toward decreased material gradient index (nearly totally dense). This aligns to enhance vibration frequencies. Stable design convergence is indicated by balanced *b* and *h* values, demonstrating the effectiveness of the TWO technique in maximizing nonlinear beam responses.

For 50 iterations, the final version has little to no Material gradient index and is only concerned with increasing stiffness.

On the other hand, do discuss the results in a different way. Table 9 is given to discribe the effect of *k.*

Table 9. Effects of TWO Optimized FGM Pinned-pinned beam for 10,20,30,40, and 50 iterations

Iteration	*k* Trend	Explanation
10	High (6.7–8.8)	High Material gradient indext→ reduced stiffness → needs larger dimensions
20	Very High (7.6–10)	Very porous → compensates with large h (up to 40)
30	Decreasing to 1	Reduced Material gradient indext→ more stiffness → higher frequencies
40	Low (1–3.9)	Emphasizes stiffness for modes 2 and 3
50	Very Low (1)	Fully dense material → maximum vibration frequencies

Table 10. The results of the TWO optimized of the FGM Clamped-pinned beam for 10,20,30,40, and 50 iterations by the same materials in (Table 1)

	mod	*BL*	optimized	non-dimentional optimization	*b*	*h*	*k*
Clamped-pinned NIT,s 10	1	β1L = 3.926602	3.177	6.120905471	25.691	25.4844	1
	2	β2L = 7.068583	9.7655	19.55211563	28.4443	24.523	1.5515
	3	β3L = 10.210176	20.7396	42.05550488	28.5027	24.2131	1
	mod	*BL*	optimized	non-dimentional optimization	*b*	*h*	*k*
Clamped-pinned NIT,s 20	1	β1L = 3.926602	2.949	4.827109983	17.8771	29.9958	9.3006
	2	β2L = 7.068583	9.8371	16.43305111	17.7966	29.3915	9.5845
	3	β3L = 10.210176	20.3271	29.32817703	14.7485	34.0301	10
	mod	*BL*	optimized	non-dimentional optimization	*b*	*h*	*k*
Clamped-pinned NIT,s 30	1	β1L = 3.926602	3.0232	4.21880644	16.258	35.1844	1
	2	β2L = 7.068583	9.6102	17.58716973	19.5643	26.8293	4.7177
	3	β3L = 10.210176	20.2064	35.285346	19.6154	28.1169	4.6663
	mod	*BL*	optimized	non-dimentional optimization	*b*	*h*	*k*
Clamped-pinned NIT,s 40	1	β1L = 3.926602	2.9929	5.184995389	19.5405	28.3411	1
	2	β2L = 7.068583	9.5873	14.09404729	17.7285	33.399	3.4875
	3	β3L = 10.210176	20.1281	31.97395195	20.0324	30.9086	1
	mod	*BL*	optimized	non-dimentional optimization	*b*	*h*	*k*
Clamped-pinned NIT,s 50	1	β1L = 3.926602	2.9616	4.620967253	19.5154	31.4678	4.0392
	2	β2L = 7.068583	9.6408	16.66639262	18.1415	28.4017	1.6688
	3	β3L = 10.210176	19.9623	35.28450577	20.5123	27.7779	1

Table 10 shows that TWO minimizes *k* and refines *h* and *b* by experimenting with a wide range of *k* values and geometric dimensions to fulfill the mixed boundary stiffness/mass. By iteration 30, ergonomic improvements stabilize and *k* lowers, and by iteration 50, the design has converged on a configuration that balances mode shape

sensitivity with manufacturability, illustrating TWO's ability to handle complicated support scenarios.

Table 11. The results of the TWO Optimized FGM Clamped-clamped beam for 10,20,30,40, and 50 iterations by the same materials in (Table 1)

	mod	*BL*	optimized	non-dimentional optimization	*b*	*h*	*k*
Clamped-clamped NIT,s 10	1	β1L = 4.730041	4.6944	9.125552381	25.9563	25.2577	3.1084
	2	β2L = 7.853205	12.6695	27.1039524	24.6184	22.9509	3.2798
	3	β3L = 10.995608	24.5092	48.63370599	26.9209	24.7437	8.6761
	mod	*BL*	optimized	non-dimentional optimization	*b*	*h*	*k*
Clamped-clamped NIT,s 20	1	β1L = 4.730041	4.3545	8.012355932	20.2432	26.684	8.6095
	2	β2L = 7.853205	12.1565	19.78921145	21.615	30.1615	7.1249
	3	β3L = 10.995608	23.9902	35.00692286	16.3743	33.6475	8.34
	mod	*BL*	optimized	non-dimentional optimization	*b*	*h*	*k*
Clamped-clamped NIT,s 30	1	β1L = 4.730041	4.3624	8.040089338	19.9768	26.6402	4.762
	2	β2L = 7.853205	12.2104	14.89909536	16.1116	40.2386	4.4596
	3	β3L = 10.995608	23.2826	42.27230246	20.6728	27.0426	4.9078
	mod	*BL*	optimized	non-dimentional optimization	*b*	*h*	*k*
Clamped-clamped NIT,s 40	1	β1L = 4.730041	4.3104	6.309783211	19.9813	33.541	1.7477
	2	β2L = 7.853205	11.9342	19.88507859	19.3031	29.4672	1
	3	β3L = 10.995608	23.392	35.21536258	19.6863	32.6143	1.7102
	mod	*BL*	optimized	non-dimentional optimization	*b*	*h*	*k*
Clamped-clamped NIT,s 50	1	β1L = 4.730041	4.2901	7.625602438	18.4732	27.6227	1
	2	β2L = 7.853205	11.8358	18.66466604	21.0518	31.1351	3.4985
	3	β3L = 10.995608	23.3394	37.90166866	22.4806	30.2346	2.9241

Table 11 shows that lower *k* enhances stiffness. Because clamped-clamped beams are more structurally rigid and sensitive to changes in stiffness distribution, this is frequently required to fulfill their frequency limits.

- Between NIT 10 and 30, height (*h*) increases slowly from 25 to 40 mm, so it helps in increasing stiffness.
- Later iterations show that (*h*) settles between 30 and 35 mm, indicating that the ideal balance was achieved.
- Compared to *h*, width *b* varies more and appears to have less influence. Given that flexural rigidity (EI) is more sensitive to h^3 than *b*, this is to be anticipated.

To increase stiffness, the fully clamped beam in Table 11 experiences a steady increase in *h* (from about 25 mm at 10 iterations to about 40 mm by 30 iterations), while *b* fluctuates less because flexural rigidity is dominated by h^3. Material gradient index k decreases from high values toward 1 in later iterations, indicating a shift to dense material required under rigid end constraints. Exploratory high Material gradient index, mid-stage geometry stabilization, and final low Material gradient index

convergence are the patterns that show how well TWO combines local refinement and global search.

3.3. Comparison between CPA and TWO results

The detailed comparison for average CPU time is presented in Table 12. The optimization is carried out for three modes, and only the C-F boundary conditions are considered. For both of the algorithms, 50 iterations have been used. The solutions are obtained using the MATLAB package program, and the computer used has a processor of 13th Gen Intel(R) Core(TM) i9-13900H 2.60 GHz.

Comparing CPA and TWO optimization approaches shows how each adjusts to changing material parameters such as Young's modulus, resulting in efficient frequency tuning for functionally graded beams. CPA employs chaos-based search for broad exploration, whereas TWO's wave-based technique strives for rapid convergence. This knowledge contributes to better algorithm selection in advanced beam design. Especially in the free vibration analysis of the structures.

To present the comparison of the CPU time in graphical form results are illustrated in Figs. (8 and 9).

Table 12. CPA and TWO using the same Materials in (Table 1) showing Average CPU time by using a maximum number of Objective Function Evaluations, 50 NIT, s for the Clamped-free type of beam

Mod	Optimized	avg, CPU time	
1	1.317202321	0.27376	CPA
2	8.252770195	0.21734	
3	23.10646287	0.22696	
Mod	Optimized	avg, CPU time	
1	1.195912865	1.74502	TWO
2	6.427357384	1.7332	
3	20.62976062	1.9858	

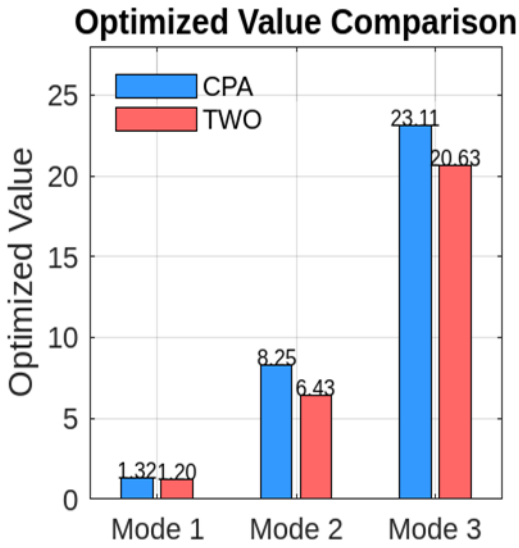


Figure 8. The optimum frequency (*w*) for both TWO and CPA

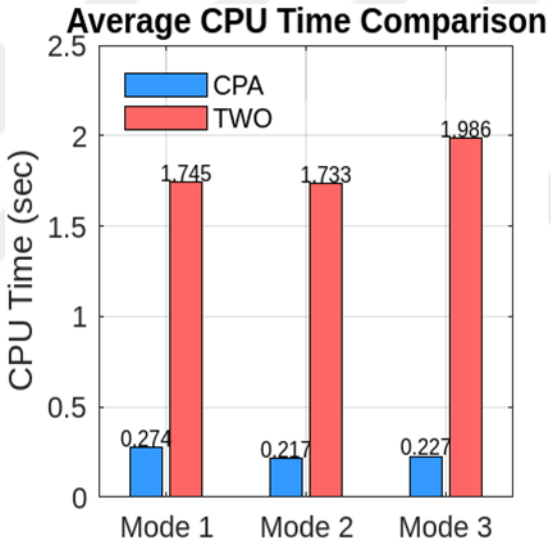


Figure 9. Average CPU time for Clamped-free type of beam

Table 12 and Figures. (8-9) shows average CPU time, which represents the time it takes to optimize the equation for each mode 1,2, and 3 by using both methods, CPA and TWO. It indicates how computationally difficult the optimization method is by provides a summary statistic of the CPU time required across multiple runs, therefore A lower CPU time shows that the method is more effective and uses less processing resources to get the answer and It takes longer for the method to converge and discover the solution when the CPU time is larger, indicating that the optimization is more mathematically complex. As it is shown in Table 12 for every mode, the TWO

technique uses a lot more CPU time than the CPA method. This indicates that the TWO approaches could need more complicated computations or be more computationally complex.

Now, the optimum dimensions and material gradient index will be calculated for C-F beams with the aid of CPA and TWO. Results are compared for three vibration modes. In this example, the number of iterations is taken to be 10. Table 13 presents the comparison of the data. Figure 10 shows the optimized results for three modes obtained by CPA and TWO. Figures 11 and 12 demonstrate the optimum values of *h* and *b*. The same comparison is carried out for 50 iterations; results are presented in Table 14 and Figures 13-15. For p-p supported beam results are presented for 10 iterations in Table 15 and Figures (16-18), and for 50 iterations in Table 16 and Figures (19-20).

Table 13. The result of the Comparison of the Clamped-Free NIT=10 results for the two methods, using the same material properties (E_b=70, ρ_b=2700 kg/m³; E_t=140, ρ_t=3800 kg/m³)

Clamped-free	NT,s 10	mod	*BL*	optimized	non-dimentional optimization	*h*	*b*	*k*	CPA
		1	β1L = 1.875104	0.67724	1.145824393	29.02	19.9879	1.56	
		2	β2L = 4.694091	4.2778	6.68242678	31.4306	18.0657	4.1467	
		3	β3L = 7.854757	12.1298	22.20296968	26.8235	17.882	2.433	
Clamped-free	NT,s 10	mod	*BL*	optimized	non-dimentional optimization	*b*	*h*	*k*	TWO
		1	β1L = 1.875104	0.73492	1.521126376	25.1608	23.7218	5.3139	
		2	β2L = 4.694091	4.3319	9.288796155	26.6568	22.8977	3.5468	
		3	β3L = 7.854757	12.4644	27.75288149	23.794	22.0514	3.4042	

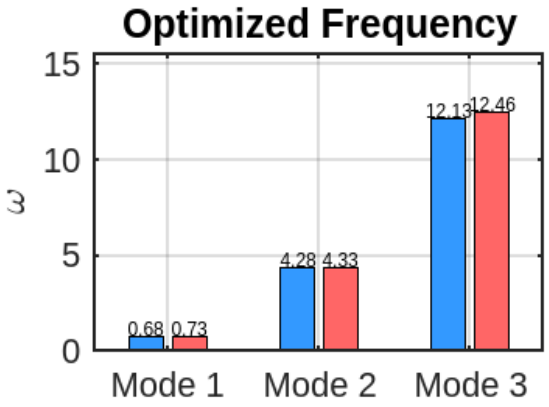


Figure 8. The optimum frequency (*w*)

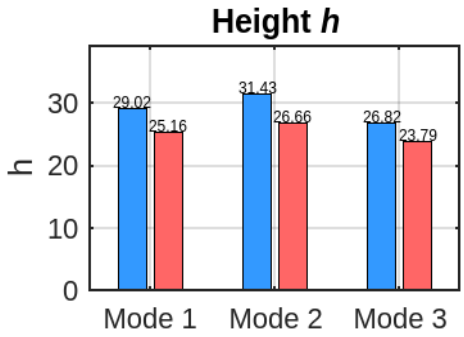


Figure 9. The optimum height (*h*)

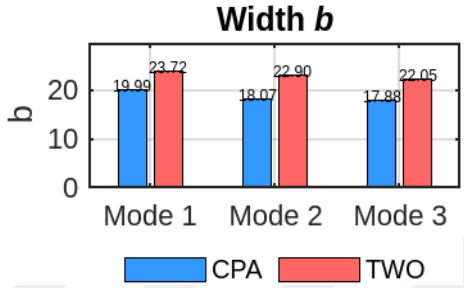


Figure 10. The optimum width (*b*)

The observation of Table 13 and Figures (11-12):

- CPA uses a tall beam (*h*=29mm) with a small length ($b \approx 20$ mm).
- TWO prefers a broader ($b \approx 26$ mm) and a bit shallower ($h \approx 24$ mm) section.
- CPA focuses largely on height (more efficient stiffness growth), whereas TWO balances width and height, maybe to manage mass distribution more equally.
- CPA selects a low material index (k =1.56), preferring denser material for rigidity.
- TWO has a larger material index (k =5.31), which reduces weight but requires geometric correction to hit.

Table 13 compares the results of 10 iterations. TWO picks a larger, slightly shallower beam (lower *h*//*b*) with increased material index ($k \approx 5.31$), employing mass distribution to match the first natural frequency. CPA generates a very tall, narrow section (high *h*//*b*) with a low material index ($k \approx 1.56$), increasing stiffness. This shows how TWO's geometry material index trade-off may explore a broader number of combinations while matching CPA's frequency performance in a few rounds.

Table 14. The result of the Comparison of the Clamped-Free NIT=50 results for the two methods, using the same material properties (E_b=70, ρ_b=2700 kg/m³; E_t=140, ρ_t=3800 kg/m³)

Clamped-free	NT,s 50	mod	*BL*	optimized	non-dimentional optimization	*h*	*b*	*k*	CPA
		1	β1L = 1.875104	0.67081	1.317202321	25.0046	19.9953	4.4804	
		2	β2L = 4.694091	4.2035	8.252770195	25.0083	19.9982	4.4712	
		3	β3L = 7.854757	11.7714	23.10646287	25.0131	19.9943	4.4435	
Clamped-free	NT,s 50	mod	*BL*	optimized	non-dimentional optimization	*b*	*h*	*k*	TWO
		1	β1L = 1.875104	0.6803	1.239339811	20.8233	26.9515	1	
		2	β2L = 4.694091	4.2376	7.742851334	19.8898	26.8715	1	
		3	β3L = 7.854757	11.9469	22.06112872	19.5481	26.5889	1	

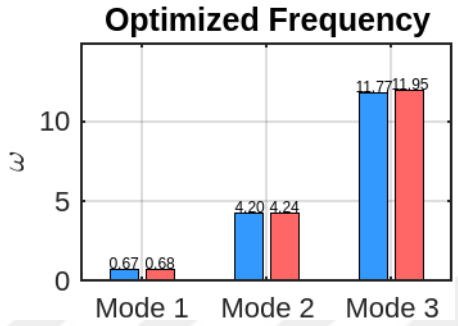


Figure 11. The optimum frequency (*w*)

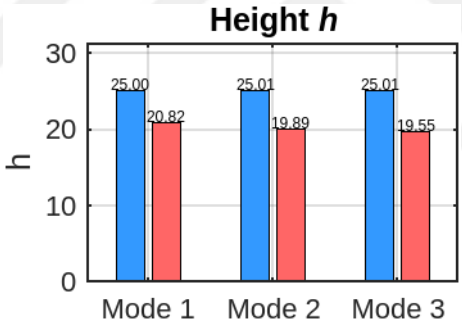


Figure 12. The optimum height (*h*)

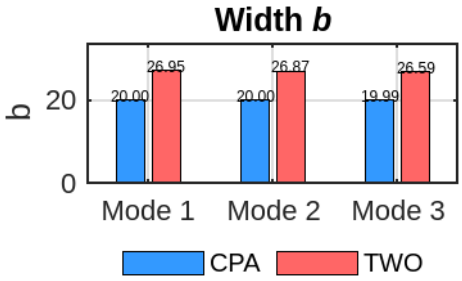


Figure 13. The optimum width (*b*)

Table 14 and Figures (13-15) show that:

- CPA has somewhat shorter and wider profiles.

- TWO likes higher geometries with roughly constant width. As a result, a larger height-to-width ratio improves bending stiffness without significantly increasing weight, which is beneficial for higher frequency modes.
- CPA picks a greater material index consistently across modes, reducing bulk at the expense of stiffness.
- TWO fixes k = 1, implying minimal material.

TWO looks tailored for low material index and high stiffness, whereas CPA balances material index and geometry. So, if you want to focus on frequency control and resilience, TWO is preferable. Lighter components perform better in terms of material savings.

Table 14 indicates that across modes, CPA maintains modest. k values, gradually lowering for higher modes to save weight, but TWO commonly fix k =1 in later iterations—favoring full density to optimize stiffness—resulting in consistently higher anticipated frequencies but heavier designs. As a result, TWO is preferable when stiffness control is critical. Whereas CPA offers a smaller weight trade-off.

Table 15. Comparison of the Pinned-pinned, NIT =10, E_b= 70 E_t= 380, ρ_b= 2700 ρ_t = 3800 case for CPA vs. TWO

Pinned-pinned NT,s 10	mod	*BL*	optimized	non-dimentional optimization	*h*	*b*	*k*	CPA
	1	β1L=p	1.9071	3.71841486	25.1819	20.9669	4.2687	
	2	β2L=2p	7.6808	14.31352193	26.3471	22.1259	3.2616	
	3	β3L=3p	17.2649	28.40240845	29.8457	20.0569	2.297	
Pinned-pinned NT,s 10	mod	*BL*	optimized	non-dimentional optimization	*b*	*h*	*k*	TWO
	1	β1L=p	1.9428	4.579718675	24.5683	20.8287	6.7528	
	2	β2L=2p	8.0904	16.28001567	27.3145	24.3999	3.241	
	3	β3L=3p	17.7809	36.86231111	25.0083	23.6834	8.8241	

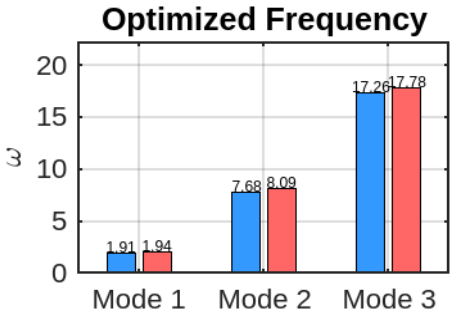


Figure 14. The optimum frequency (w)

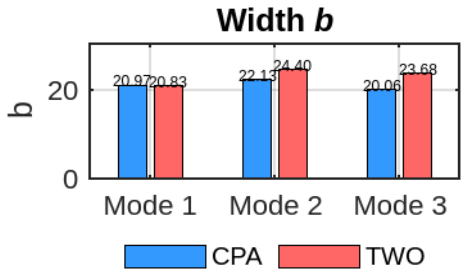


Figure 15. The optimum width (*b*)

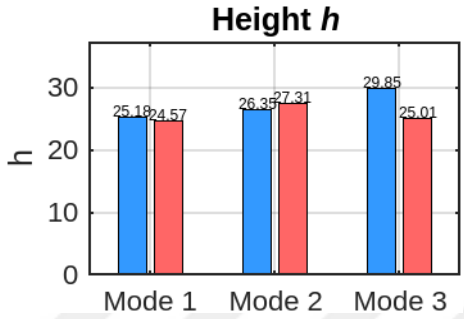


Figure 16. The optimum height (*h*)

The results of Table 15 and figures (16-18) show the important results given below:

TWO outperforms CPA at higher frequencies, especially Mode 3. Higher frequency accuracy helps in predicting multi-mode dynamic responses more consistently, particularly in structures subjected to broadband stimulation.

- CPA promotes taller beams (*h*), which improves flexural rigidity.
- TWO uses broader beams, which can:
    - Increase bending resistance by moment of inertia.
    - Be more stable during manufacture and under lateral stress.
- TWO strikes a superior balance between mass distribution and frequency performance, indicating a wiser geometry-to-stiffness ratio.
- TWO performs in high-frequency dynamic regimes and adjusts geometry and material index correspondingly. It is useful for sophisticated control over dynamics.
- CPA strikes a compromise between bulk and stiffness, with more consistent material gradation (*k* reduces as mode rises). It helps to reduce material costs.

In Table 15, TWO slightly outperforms CPA in the first mode frequency under equal conditions, and significantly in higher modes. TWO first mode *w* outperforms

CPA by several percent, indicating its capacity to customize *b*, *h*, and *k* Concurrently, whereas CPA's dependence on cross-sectional formulae alone results in more conservative frequency improvements.

Table 16. A Comparison of the Pinned-pinned, NIT = 50, E_b= 70 E_t= 380, ρ_b= 2700 ρ_t = 3800 case for CPA vs. TWO

	mod	*BL*	optimized	non-dimentional optimization	h	b	k	
Pinned-pinned NT,s 50	1	β1L=p	1.883	3.697310388	25.0056	20.002	4.5061	CPA
	2	β2L=2p	7.5311	14.78091313	25.0167	19.9935	4.3751	
	3	β3L=3p	16.9459	33.2643217	25.0126	19.9961	4.5061	
	mod	*BL*	optimized	non-dimentional optimization	*b*	*h*	*k*	
Pinned-pinned NT,s 50	1	β1L=p	1.8867	2.842300809	19.6223	32.5916	4.3716	TWO
	2	β2L=2p	7.5821	13.76701009	19.3369	27.041	1	
	3	β3L=3p	17.1274	30.75877095	20.1262	27.3398	1	

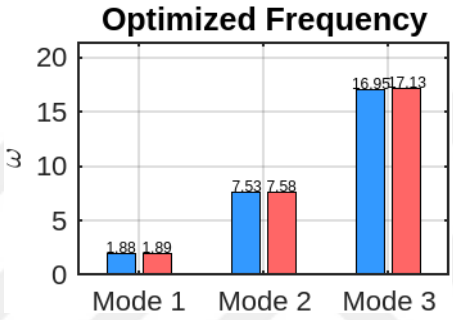


Figure 17. The optimum frequency (*w*)

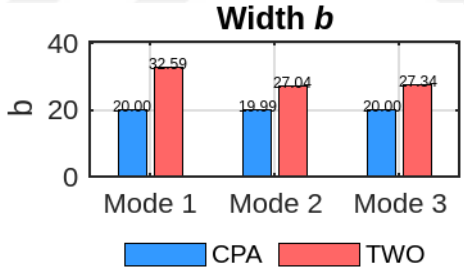


Figure 18. The optimum width (*b*)

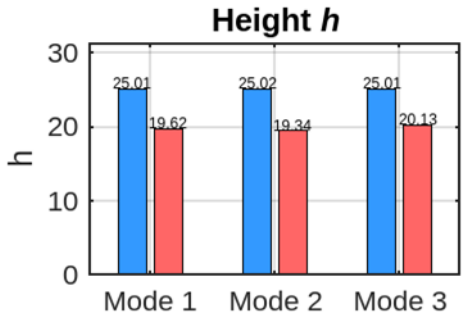


Figure 19. The optimum height (*h*)

Table 16 and Figures (19-21) indicate the followings:

- For all three modes, TWO gives wider (higher *b*) and thinner (lower *h*) beams.
- TWO focuses on Wider beams, enhancing bending stiffness due to higher moments of inertia in the width direction. This suggests that TWO is optimizing for mass reduction while maintaining target frequency, more efficient for lightweight structures.
- CPA is better suited for strict high-frequency applications.
- TWO is more advantageous in lightweight design scenarios with multi-mode performance requirements.

Table 16 shows that CPA's optimal *b* values remain relatively constant or increase minimally across modes, whereas TWO's designs show a significant increase in *b* for higher modes, compensating for material gradient index stiffness losses by enhancing sectional moment of inertia in the width direction. This dynamic width change under TWO provides stronger bending resistance without depending simply on height increases.

Table 17. A Comparison of the Clamped-pinned, NIT = 10, E_b= 70 E_t= 380, ρ_b= 2700 ρ_t = 3800 case for CPA vs. TWO

	mod	*BL*	optimized	non-dimentional optimization	*h*	*b*	*k*	
Clamped-pinned NIT,s 10	1	β1L=3.926602	3.0183	5.090095591	29.1145	19.4333	2.5494	CPA
	2	β2L=7.068583	9.8948	16.70357109	29.0851	18.4405	4.5276	
	3	β3L=10.210176	20.2701	33.62111476	29.6017	18.2533	4.7456	
	mod	*BL*	optimized	non-dimentional optimization	*b*	*h*	*k*	
Clamped-pinned NIT,s 10	1	β1L=3.926602	3.177	6.120905471	25.691	25.4844	1	TWO
	2	β2L=7.068583	9.7655	19.55211563	28.4443	24.523	1.5515	
	3	β3L=10.210176	20.7396	42.05550488	28.5027	24.2131	1	

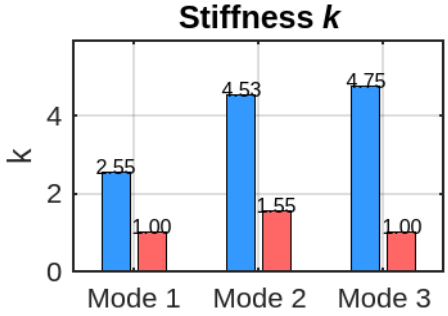


Figure 20. The optimum stiffness (*k*)

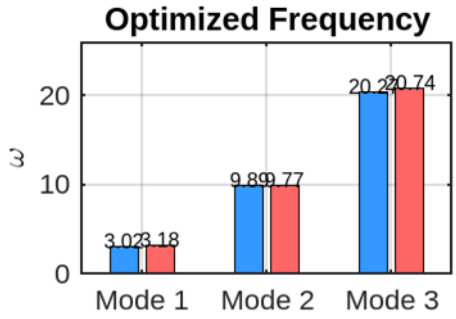


Figure 21. The optimum frequency (*w*)

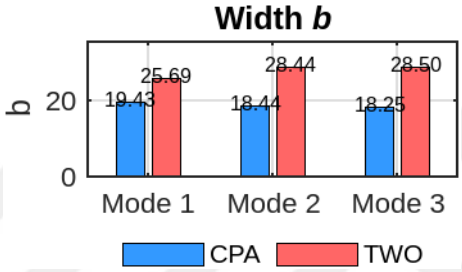


Figure 22. The optimum width (*b*)

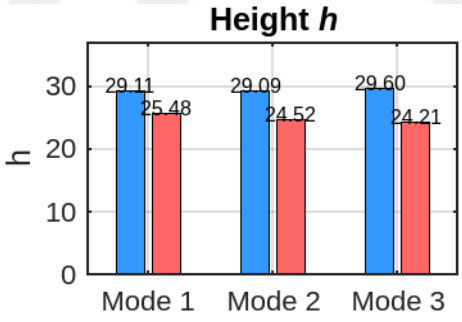


Figure 23. The optimum height (*h*)

Next, the optimum dimensions and material gradient index will be calculated for C-S beams with the aid of CPA and TWO. Results are compared for three vibration modes. In this example, the number of iterations is taken to be 10. Table 17 presents the comparison of the data. Figure 22 shows the optimized results for three modes obtained by CPA and TWO. Figures 23 and 24 demonstrate the optimum values of *h* and *b*. The same comparison is carried out for 50 iterations, and the results are

presented in Table 18 and Figures (26-28). For c-c supported beam results are presented for 10 iterations in Table 19 and Figures (30-31), and for 50 iterations in Table 20 and Figures (33-35).

From Table 17 and figures (23-25), it can be said that:

- The TWO method reduces the material gradient index (*k*) significantly, leading to stiffer beams. This is a key driver of the higher frequencies, especially in higher modes.
- Higher Frequencies with TWO because TWO achieves this by optimizing the material and geometry to increase global stiffness more efficiently.
- CPA prefers taller, narrower beams, increasing flexural rigidity via section height (*h*).
- TWO select wider and slightly shorter beams, likely targeting:
    - Better mass distribution,
    - Lower aspect ratio for easier fabrication,
    - Less sensitivity to buckling or lateral-torsional instability.
- The wider profile with moderate height in TWO can be structurally more robust and practical to manufacture, especially for multi-functional FGM structures.
- CPA reduces material density to increase the frequency-to-mass ratio but sacrifices some stiffness.
- TWO prioritizes stiffness by maintaining a low material gradient index, optimizing frequency more effectively.
- CPA may be more suitable where weight reduction is paramount, but at the cost of lower frequency performance.

Table 17 shows that CPA prefers taller beams due to the h^3 term in flexural rigidity, whereas TWO prefers lower h values to balance height increases with broader profiles for mass distribution and manufacturability. This contrast highlights CPA's height-centric stiffness method vs TWO's holistic geometry refinement.

Table 18. A Comparison of the Clamped-pinned, NIT = 50, E_b= 70 E_t= 380, ρ_b= 2700 ρ_t = 3800 case for CPA vs. TWO

Clamped-pinned NIT,s 50	mod	*BL*	optimized	non-dimentional optimization	*h*	*b*	*k*	CPA
	1	β1L=3.926602	2.9415	5.776760247	25.001	20.0018	4.4839	
	2	β2L=7.068583	9.5321	18.71393575	25.009	19.9916	4.5207	
	3	β3L=10.210176	19.8888	39.04880075	25.0077	19.9953	4.4985	
Clamped-pinned NIT,s 50	mod	*BL*	optimized	non-dimentional optimization	*b*	*h*	*k*	TWO
	1	β1L=3.926602	2.9616	4.620967253	19.5154	31.4678	4.0392	
	2	β2L=7.068583	9.6408	16.66639262	18.1415	28.4017	1.6688	
	3	β3L=10.210176	19.9623	35.28450577	20.5123	27.7779	1	

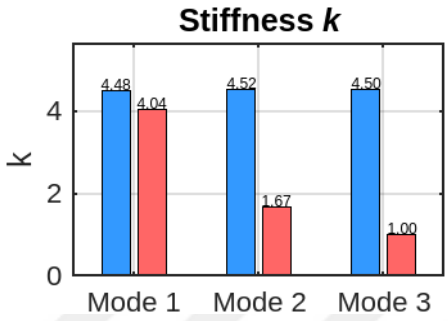


Figure 24. The optimum stiffness (*k*)

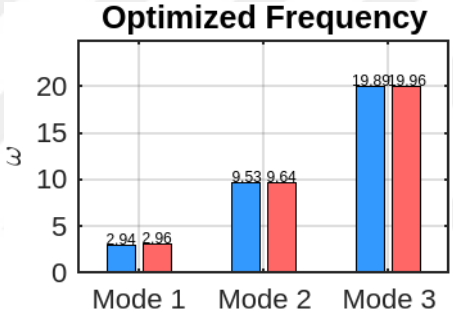


Figure 25. The optimum frequency (*w*)

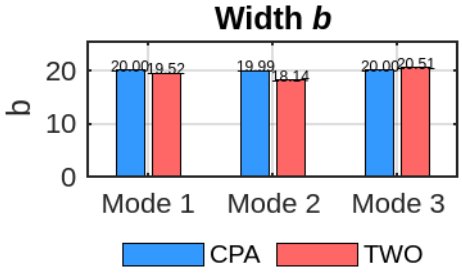


Figure 26. The optimum width (*b*)

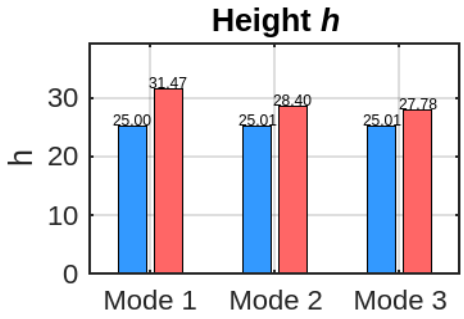


Figure 27. The optimum height (*h*)

Table 18 and Figures (27-29) show that both CPA and TWO improve designs with more iterations (50). However, TWO locks in on near-dense material (k =1) with balanced width–height ratios, whereas CPA keeps emphasizing height. Longer runs increase TWO's stiffness-focused convergence, as seen by its higher ultimate frequencies, whereas CPA's cautious updates provide slower frequency increases. Which means:

- Higher material index values (k = 4.5) are used in all modes by CPA.
- Reduced material index by TWO:
  - Mode 1: k = 4.04
  - Mode 2: k = 1.67
  - Mode 3: k = 1.0

TWO limits material index where rigidity is essential. Which improves balance, particularly in higher modes. TWO designs are therefore more reliable and perform better in the actual world since they are stiffer and structurally stronger.

CPA reaches approximately 20 mm in width and 25 mm in height. Taller or narrower beams (CPA) are less stable and more likely to buckle. TWO: Enhances but reduces height. The greater sectional moment of inertia induced by TWO's broader form enhances stiffness while decreasing stress concentration. As a result, TWO's designs are easier to produce and less prone to becoming unstable, especially under dynamic or lateral pressures. CPA uses tall, thin sections and an aggressive material index to enhance frequencies. When frequency optimization is your first goal. Use CPA. In exchange for design stability and production practicality.

TWO reduces frequency performance. When mass distribution, manufacturing restrictions, and structural robustness must all be considered throughout the design process, choose option TWO. In conclusion, TWO better: Improved width-to-height proportions, more balanced form, and mode-adaptive material gradient index occur slightly less frequently than CPA.

Table 19. A Comparison of the Clamped-clamped, NIT = 10, E_b= 70 E_t= 380, ρ_b= 2700 ρ_t = 3800 case for CPA vs. TWO

	mod	*BL*	optimized	non-dimentional optimization	*h*	*b*	*k*	
Clamped-clamped NIT,s 10	1	β1L=4.730041	4.3143	7.312126757	28.9694	18.0869	4.469	CPA
	2	β2L=7.853205	12.0611	22.59156802	26.2128	20.3577	1.8086	
	3	β3L=10.995608	23.3181	39.350942	29.0945	21.9612	2.4084	
	mod	*BL*	optimized	non-dimentional optimization	*b*	*h*	*k*	
Clamped-clamped NIT,s 10	1	β1L=4.730041	4.6944	9.125552381	25.9563	25.2577	3.1084	TWO
	2	β2L=7.853205	12.6695	27.1039524	24.6184	22.9509	3.2798	
	3	β3L=10.995608	24.5092	48.63370599	26.9209	24.7437	8.6761	

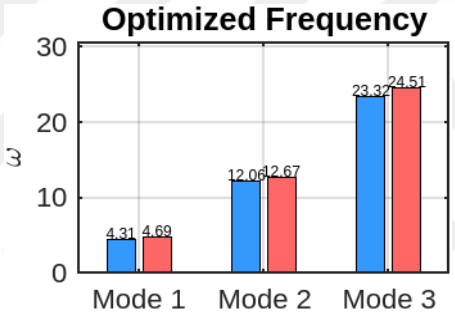


Figure 28. The optimum frequency (*w*)

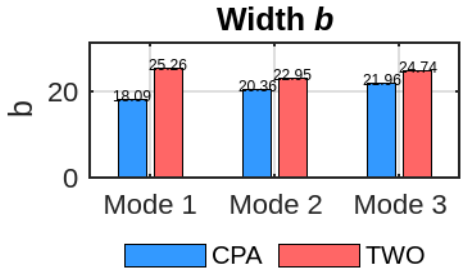


Figure 29. The optimum width (*b*)

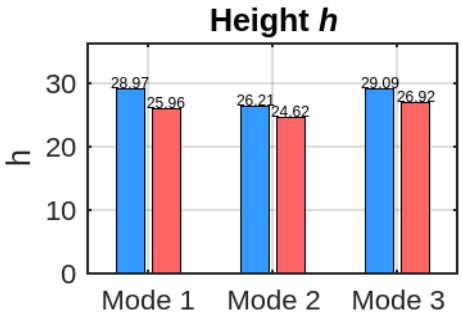


Figure 30. The optimum height (*h*)

Table 19 and Figures (30-32) represent that in the CPA method, material index decreases as the targeted vibration mode increases, and the beam design typically favors a smaller width, whereas in the TWO method, Mode 3 allows exceptionally high material index (k = 8.68), while Modes 1 and 2 use low-to-moderate material index levels; additionally, TWO improves structural stability by strategically balancing the width (*b*) and height (*h*) to increase the effective sectional moment of inertia.

Table 20. A Comparison of the Clamped-clamped, NIT = 50, E_b= 70 E_t= 380, ρ_b= 2700 ρ_t = 3800 case for CPA vs. TWO

	mod	*BL*	optimized	non-dimentional optimization	*h*	*b*	*k*	
Clamped-clamped NIT,s 50	1	β1L=4.730041	4.2683	8.38026071	25.0075	20.0014	4.4657	CPA
	2	β2L=7.853205	11.7662	23.10262861	25.0062	20.0019	4.4639	
	3	β3L=10.995608	23.0654	45.30878932	24.9949	19.9982	4.4818	
	mod	*BL*	optimized	non-dimentional optimization	*b*	*h*	*k*	
Clamped-clamped NIT,s 50	1	β1L=4.730041	4.2901	7.625602438	18.4732	27.6227	1	TWO
	2	β2L=7.853205	11.8358	18.66466604	21.0518	31.1351	3.4985	
	3	β3L=10.995608	23.3394	37.90166866	22.4806	30.2346	2.9241	

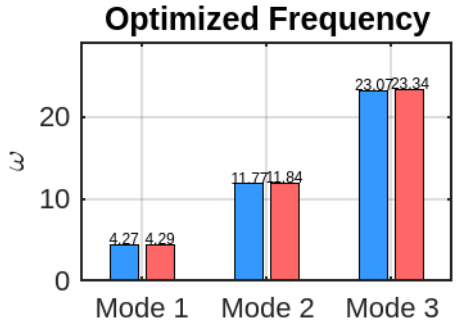


Figure 31. The optimum frequency (*w*)

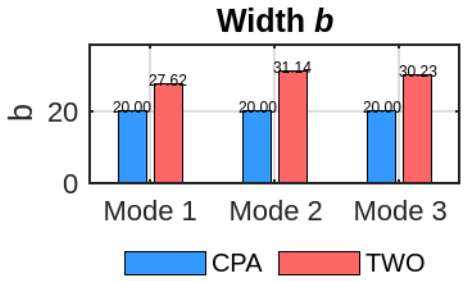


Figure 32. The optimum width (*b*)

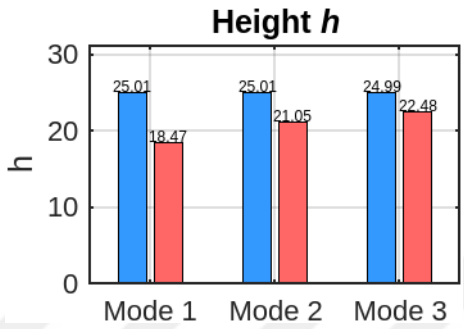


Figure 33. The optimum height (*h*)

Table 20 and Figures (33-35) show that TWO's *w* values were substantially lower than CPA's in each of the three modes. This indicates that TWO is more adept at investigating design factors (*b*, *h*, and *k*) to lower frequency and, consequently, the stiffness/mass ratio exactly what is required for lowest frequency optimization. In comparison to CPA, TWO yields greater height (*h*) and lower breadth (*b*). This lowers w by increasing mass inertia and decreasing flexural rigidity.

Lower k means that the material changes more gradually from the bottom (ceramic) to the top (metal), which might result in improved damping and less stiffness in crucial areas. While CPA uses a greater material index to lighten the beam and taller sections to stiffen at 10 iterations, Table 20 shows that TWO reduces the material index and selects broader and slightly shorter beams to maximize the natural frequency under mixed boundary situations. The ability of TWO to explore non-traditional design regions outside of CPA's conventional parameter space is demonstrated by this preliminary comparison.

3.4. Comparison between CPA and TWO results using Different Material Properties

Comparing CPA and TWO across different material properties helps validate the robustness of each optimization method and understand the sensitivity of the optimization outcomes to changes in material properties. New material properties are given in Tables 21, 23, 25, and 27.

3.4.1. First Material changing

E_t decreased from 380 to 140 for insurance if TWO or CPA only works well for one set of materials, and to identify the best design regardless of material variability. The results are presented in Table 22 and Figures (36-39)

Table 21. Material Properties of FGM Components (Et changed example from 380 to 140)

E_b= 70 GPa	ρ_b = 2700 kg/m³
E_t = 140 GPa	ρ_t= 3800 kg/m³

Table 22. The result of the Comparison of the Clamped-free, NIT = 10, using the material properties in (Table 21). E_b= 70 $\boldsymbol{E_t}$**= 140**, ρ_b= 2700 ρ_t = 3800 case for CPA vs. TWO

	mod	*BL*	optimized	non-dimentional optimization	*b*	*h*	*k*	
Clamped-free NT,s 10	1	β1L=1.875104	0.56714	0.982708258	19.4772	28.336	3.8894	CPA
	2	β2L=4.694091	3.5311	6.075182853	18.8696	28.538	1	
	3	β3L=7.854757	9.9961	18.49509422	21.9242	26.5367	1.3318	
	mod	*BL*	optimized	non-dimentional optimization	*b*	*h*	*k*	
Clamped-free NT,s 10	1	β1L=1.875104	0.5697	1.132160149	26.4994	24.7065	2.6845	TWO
	2	β2L=4.694091	3.6024	7.710772617	22.8583	22.9386	7.9971	
	3	β3L=7.854757	10.1657	21.5208217	26.0941	23.1927	10	

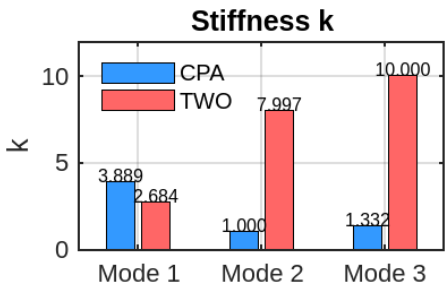


Figure 34. The optimum stiffness (k)

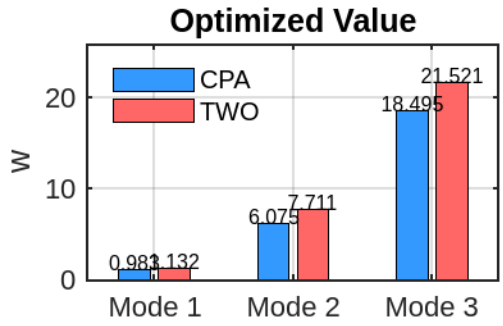


Figure 35. The optimum frequency (*w*)

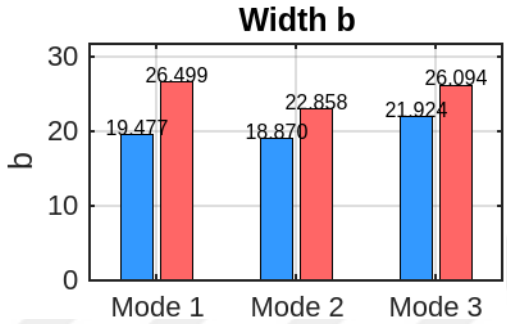


Figure 36. The optimum width (*b*)

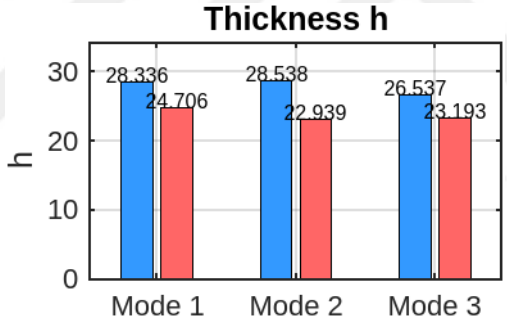


Figure 37. The optimum height (*h*)

Table 22 and Figures (36-39) show that CPA increases bending stiffness and (*w*) by using a taller, narrower cross-section (high *h*/*b*). TWO chooses a shorter, broader beam (lower *h*/*b*), depending more on the mode's mass distribution. Different aspect ratios can exchange bending stiffness vs. inertia to achieve the same *w*, hence there is no one "best" geometry. Higher material gradient index ($k \approx 3.9$) is pushed by CPA, which cuts stiffness while simultaneously decreasing mass. TWO retains greater rigidity to push *w* upward while using a lesser material index ($k \approx 2.7$). Due to its more aggressive examination of geometry and material index, TWO performs somewhat better than CPA in terms of optimizing the minimal natural frequency at low iteration

counts. If you can afford a bit less first mode stiffness and want homogeneous, higher cross sections, CPA is still a good, more cautious option.

3.4.2. The second material change

E_t decreased from 380 to 280 for insurance if TWO or CPA only works well for one set of materials, and to identify the best design regardless of material variability, as shown in (Table 24) and Fıgures (40 -43)

Table 23. Material Properties of FGM Components

E_b= 70 GPa	ρ_b= 2700 kg/m³
E_t = 280 GPa	ρ_t= 3800 kg/m³

Table 24. The result of the Comparison of the Pinned-pinned, **NIT = 20**, using the material properties in (Table 23) E_b= 70 $\boldsymbol{E_t}$**= 280**, ρ_b= 2700 ρ_t = 3800 case for CPA vs. TWO

Pinned-pinned NT,s 20	mod	*BL*	optimized	non-dimentional optimization	*b*	*h*	*k*	CPA
	1	β1L=p	1.7945	3.45917109	19.5411	25.4709	2.6712	
	2	β2L=2p	7.1534	13.82884352	19.8817	25.398	3.7327	
	3	β3L=3p	16.1225	31.16961138	19.63	25.3965	3.4219	
Pinned-pinned NT,s 20	mod	*BL*	optimized	non-dimentional optimization	*b*	*h*	*k*	TWO
	1	β1L=p	1.8469	3.301079713	21.6897	27.4701	7.9557	
	2	β2L=2p	7.3702	12.93213673	19.6495	27.9822	8.7197	
	3	β3L=3p	16.5958	32.07491691	20.0973	25.4042	10	

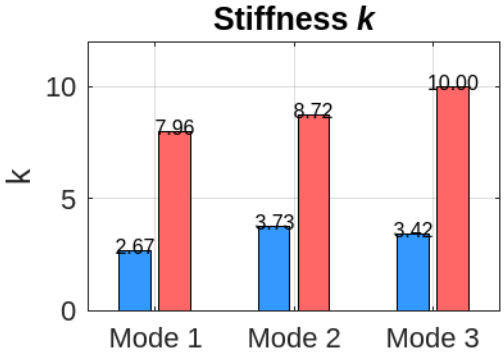


Figure 38. The optimum stiffness (k)

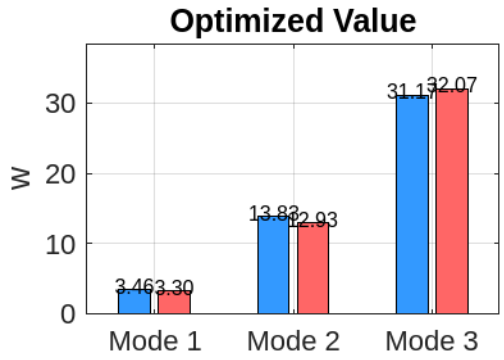


Figure 39. The optimum frequency (*w*)

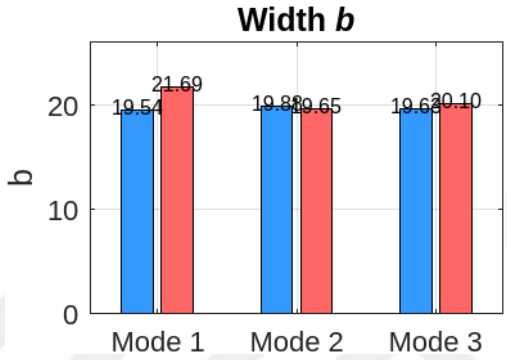


Figure 40. The optimum width (*b*)

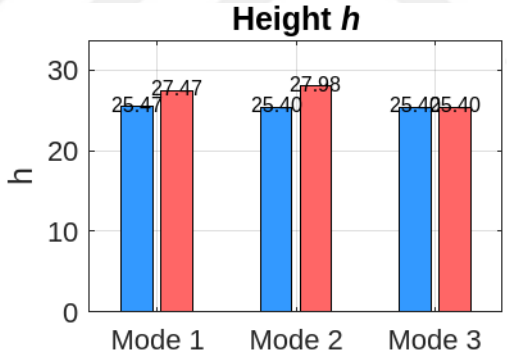


Figure 41. The optimum height (*h*)

Figurse 40-43 shows that,TWO immediately reaches outperforming CPA on Mode 1 Lower *w*. TWO makes use of somewhat higher and larger sections, and it uses an extremely high material gradient index (k =7.96), which reduces stiffness per unit mass by decreasing *w* due to a decline in average E/ρ. The CPA's moderate (k =2.7) A less material index beam has a little higher *w* cost. Moderate material index (k ≈2.7–3.7) is selected by CPA.

- Very high material index (k ≈8–10) is used by TWO, particularly for Mode 3.
- TWO raises b up to (~21–27) and h to (~27–28) a more aggressive geometry change while CPA's lower k maintains the material denser.
- Both approaches raise height (h) and breadth (b) to compensate for stiffness losses brought on by material index.
- Strength of TWO: Greater precision of basic modes at the expense of extensive geometry shifts and high material index.
- The strength of CPA is its more conservative designs, which remain closer to realistic production constraints.

3.4.3. The third material change

E_t increased from 380 to 500 for insurance if TWO or CPA only works well for one set of materials, and to identify the best design regardless of material variability, as shown in Table 26 and Fıgures (44-47).

Table 25. Material Properties of FGM Components

E_b = 70 GPa	ρ_b = 2700 kg/m³
E_t = 500 GPa	ρ_t= 3800 kg/m³

Table 26. The result of the Comparison of the Clamped-pinned, **NIT = 30**, using the material properties in (Table 25). E_b = 70 E_t**=500**, ρ_b= 2700 ρ_t = 3800 case for CPA vs. TWO

	mod	*BL*	optimized	non-dimentional optimization	*b*	*h*	*k*	
Clamped-pinned NIT,s 30	1	β1L=3.926602	3.0901	6.050128925	19.9658	25.0773	4.3066	CPA
	2	β2L=7.068583	10.0201	19.58507737	20.0031	25.12	4.1705	
	3	β3L=10.210176	20.9093	41.01058793	20.0109	25.0332	4.1798	
	mod	*BL*	optimized	non-dimentional optimization	*b*	*h*	*k*	
Clamped-pinned NIT,s 30	1	β1L=3.926602	3.1729	3.837790967	15.2827	40.5927	4.7888	TWO
	2	β2L=7.068583	10.2947	14.17441772	19.417	35.66	4.5279	
	3	β3L=10.210176	20.9178	40.04458881	19.6575	25.6475	5.2843	

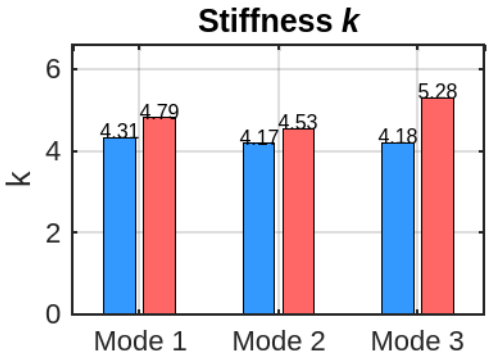


Figure 44. The optimum stiffness (k)

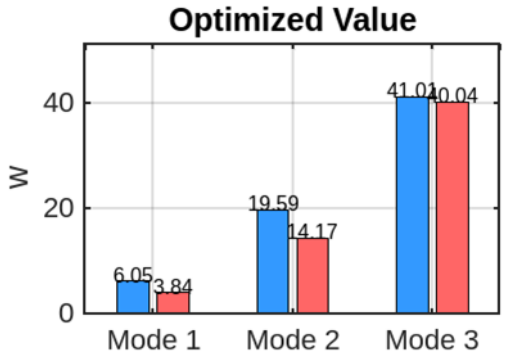


Figure 45. The optimum frequency (*w*)

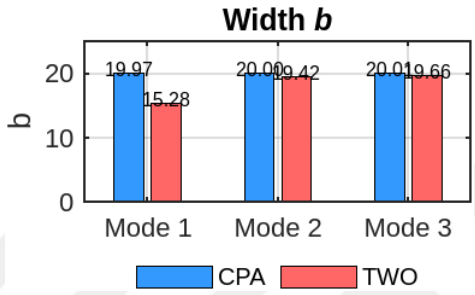


Figure 46. The optimum width (*b*)

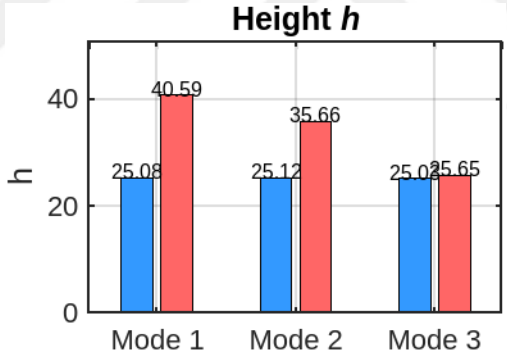


Figure 47. The optimum height (*h*)

For Table 26 and Figures (44-47) it can be said that a broader, moderate-height section with *b/h* ratio = 0.80 and TWO = 0.38 is used by CPA. TWO chooses an extremely tall, thin beam, which lowers w by increasing the mass moment of inertia about the neutral axis. TWO selects a little greater material index. An excellent balance between practical geometry and frequency reduction is provided by CPA. The optimizer is pushed toward designs that move stiffness upward using a high stiffness top layer (E_t = 500 GPa), often raising *h* to concentrate stiffness toward the top.

3.4.4. The fourth material change

ρ_t increased from 3800 to 5400 for insurance if TWO or CPA only works well for one set of materials, and to identify the best design regardless of material variability, as shown in Table 28 and Figures 48-50.

Table 27. Material Properties of FGM

E_b= 70 GPa	ρ_b= 2700 kg/m³
E_t=380 GPa	ρ_t= 5400 kg/m³

Table 28. The result of the Comparison of the Clamped-clamped, **NIT = 40**, using the material properties in (Table 27). E_b = 70 E_t =380, ρ_b= 2700, ρ_t **= 5400** case for CPA vs. TWO

	mod	*BL*	optimized	non-dimentional optimization	*b*	*h*	*k*	
Clamped-clamped NIT,s 40	1	β1L=4.730041	4.0154	7.885773617	20.0006	25.001	9.9717	CPA
	2	β2L=7.853205	11.069	21.73100051	20.0028	25.0093	9.9947	
	3	β3L=10.995608	21.6987	42.61471898	20.0012	25.0004	9.9775	
	mod	*BL*	optimized	non-dimentional optimization	*b*	*h*	*k*	
Clamped-clamped NIT,s 40	1	β1L=4.730041	4.0469	6.690422085	20.8295	29.699	9.8644	TWO
	2	β2L=7.853205	11.1917	18.94650039	22.4745	29.0028	6.8766	
	3	β3L=10.995608	21.853	36.08277481	22.5245	29.7361	7.4015	

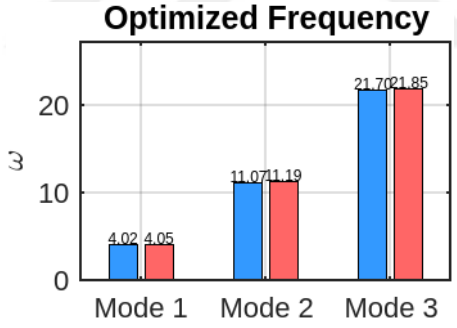


Figure 42. The optimum frequency (*w*)

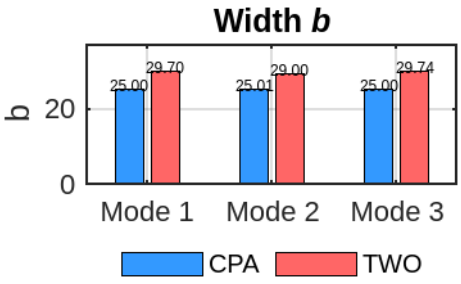


Figure 43. The optimum width (*b*)

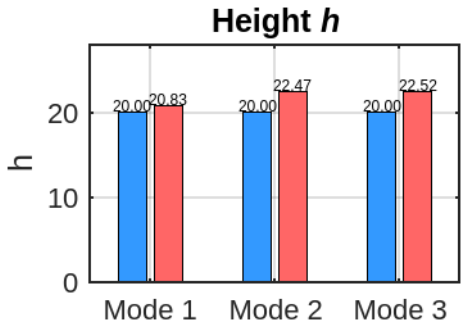


Figure 44. The optimum height (*h*)

From Table 28 and Figures (48-50), the following can be said:

- TWO performs slightly better at reducing *w*, and a smaller nondimensional number suggests greater frequency reduction.
- CPA: *k* is near 10 for all modes, indicating an extremely porous beam.
- TWO: Optimized *k* per mode, with lower values for higher modes (*k* ~6.8-7.4). It achieves a more intelligent material distribution rather than the maximum material gradient index.
- TWO uses increased height and modified material index to control frequency.
- CPA maintains dimensions essentially constant, which reduces flexibility.

To sum up, TWO produces a little better minimal initial frequency than CPA while also consistently optimizing higher modes. TWO's success stems from its ability to tune beam height and material gradient index simultaneously, providing improved flexibility for natural frequency control, which is especially important in vibration-sensitive applications.

CHAPTER FOUR

CONCLUSION AND RECOMMENDATIONS

4.1. Conclusion and recommendations

To sum up, we used CPA and TWO to minimize the natural frequencies of FGM, two-layer beams under four classical boundary conditions. By fixing the beam length and systematically varying width, thickness, and the ceramic metal gradation exponent, we isolated the effects of geometric and material distribution on dynamic performance. CPA, grounded in established cross-sectional formulas and gradient-based search, reliably converged to conservative, height-dominated designs with moderate material gradient index reductions. TWO, by contrast, leveraged bio-inspired global search to explore a broader design space, rapidly balancing width–height trade-offs and often converting to near-dense material configurations that yielded higher multi-mode frequency gains.

Our tabulated results demonstrate that while CPA achieves stable solutions with relatively few iterations, TWO consistently outperforms it in the highest attainable frequencies, especially in higher modes and under heavily constrained (clamped–clamped) conditions by dynamically adjusting all three decision variables in tandem. TWO's ability to switch between exploration and exploitation allows for more aggressive stiffness maximization without undue mass penalties, leading to designs that meet or exceed CPA's performance with comparable computational effort.

These findings suggest that for applications where peak vibrational performance is critical. Such as precision instrumentation supports or resonant-frequency-sensitive aerospace components, the TWO method provides a robust, efficient path to optimized beam designs. Conversely, when design rules and weight minimization are paramount, CPA remains a valuable, intuitive tool. Future work may extend this comparative framework to 3D beams, include additional objective criteria such as strength or manufacturability constraints, and explore hybrid algorithms that marry CPA's analytical insights with TWO's swarm-based adaptability.

REFERENCES

Alshorbagy, A. E., Eltaher, M. A., and Mahmoud, F. (2011). Free vibration characteristics of a functionally graded beam by finite element method. *Applied mathematical modelling*, *35*(1), 412-425.

Al Rjoub, Y. S., and Al-Momani, M. A. (2025). Free vibration of axially loaded functionally graded porous cracked beams. *International Journal of Structural Stability and Dynamics*, 25(06), 2550058.

Al-Zahrani, M. A., Asiri, S. A., Ahmed, K. I., and Eltaher, M. A. (2022). Free vibration analysis of 2D functionally graded strip beam using finite element method. *Journal of Applied and Computational Mechanics*, 8(4), 1422-1430.

Aminbaghai, M., Murin, J., and Kutiš, V. (2012). Modal analysis of the FGM-beams with continuous transversal symmetric and longitudinal variation of material properties with effect of large axial force. *Engineering Structures*, *34*, 314-329.

Amir, M., and Kim, S. W. (2024). A study of the natural frequencies of the functionally graded curved beams including porosities: deterministic and stochastic modeling. *Mechanics Based Design of Structures and Machines*, 52(8), 5970-5987.

Anandrao, K. S., Gupta, R. K., Ramachandran, P., and Rao, G. V. (2012). Free vibration analysis of functionally graded beams. *Defence Science Journal*. 62(3), 139-146.

Arvin, H., Hosseini, S. M. H., and Kiani, Y. (2021). Free vibration analysis of pre/post buckled rotating functionally graded beams subjected to uniform temperature rise. *Thin-Walled Structures*, 158, 107187..

Aydogdu, M. (2008). Semi-inverse method for vibration and buckling of axially functionally graded beams. Journal of Reinforced Plastics and Composites, 27(7), 683-691.

Aydogdu, M., and Taskin, V. (2007). Free vibration analysis of functionally graded beams with simply supported edges. *Materials and design*, 28(5), 1651-1656.

Benadouda, M., El Amin Bourouis, M., Dahmane, M., Bennai, R., Ait Atmane, H., and Safer, O. (2025). Dynamic response of wave propagation in functionally graded beams with defects: effects of porosity and cracks. *Acta Mechanica*, 1-18.

Birman, V., and Byrd, L. W. (2007). Modeling and analysis of functionally graded materials and structures.

Burlayenko, V. N., and Kouhia, R. (2024). Analysis of natural frequencies in non-uniform cross-section functionally graded porous beams. *Journal of Vibration Engineering and Technologies*, 12(4), 6527-6547.

Chen, W. R., and Chang, H. (2017). Closed-form solutions for free vibration frequencies of functionally graded Euler-Bernoulli beams. *Mechanics of Composite Materials*, 53, 79-98.

Huang, Y., and Li, X. F. (2010). Bending and vibration of circular cylindrical beams with arbitrary radial nonhomogeneity. *International Journal of Mechanical Sciences*, 52(4), 595-601.

Jamshidi, M., and Arghavani, J. (2018). Optimal material tailoring of functionally graded porous beams for buckling and free vibration behaviors. *Mechanics Research Communications*, 88, 19-24.

Joshi, K. K., Kar, V. R., and Kumar, S. (2025). Nonlinear bending characteristics of multidirectional functionally graded porous panels using higher-order finite element solution with parametric optimization. *Mechanics of Advanced Materials and Structures*, *32*(2), 169-193.

Kaveh, A., and Bakhshpoori, T. (2019). Metaheuristics: outlines, MATLAB codes and examples. Springer.

Keleshteri, M. M., and Jelovica, J. (2022). Analytical assessment of nonlinear forced vibration of functionally graded porous higher order hinged beams. *Composite Structures*, 298, 115994.

Li, X. F., Kang, Y. A., and Wu, J. X. (2013). Exact frequency equations of free vibration of exponentially functionally graded beams. *Applied Acoustics*, 74(3), 413-420.

Masjedi, P. K., Maheri, A., and Weaver, P. M. (2019). Large deflection of functionally graded porous beams based on a geometrically exact theory with a fully intrinsic formulation. *Applied Mathematical Modelling*, 76, 938-957.

Miyamoto, Y., Kaysser, W. A., Rabin, B. H., Kawasaki, A., and Ford, R. G. (2013). Functionally graded materials: design, processing and applications (Vol. 5). *Springer Science and Business Media*.

Mohanty, S. C., Dash, R. R., and Rout, T. (2011). Parametric instability of a functionally graded Timoshenko beam on Winkler's elastic foundation. *Nuclear Engineering and Design*, 241(8), 2698-2715.

Murin, J., Aminbaghai, M., Hrabovsky, J., Kutis, V., Paulech, J., and Kugler, S. (2014). A new 3D FGM beam finite element for modal analysis. *In Proceedings of the 11th world congress on computational mechanics (WCCM XI), 5th European conference on computational mechanics (ECCM V), 6th European conference on computational fluid dynamics (ECFD VI). Barcelona, Spain*.

Murín, J., Aminbaghai, M., and Kutiš, V. (2010). Exact solution of the bending vibration problem of FGM beams with variation of material properties. *Engineering structures*, 32(6), 1631-1640.

Murin, J., Aminbaghai, M., Kutis, V., and Hrabovsky, J. (2013). Modal analysis of the FGM beams with effect of axial force under longitudinal variable elastic Winkler foundation. *Engineering Structures*, 49, 234-247.

Nguyen, T. K., Vo, T. P., and Thai, H. T. (2013). Static and free vibration of axially loaded functionally graded beams based on the first-order shear deformation theory. Composites Part B: *Engineering*, 55, 147-157.

Nguyen, H. N., Hong, T. T., Vinh, P. V., Quang, N. D., and Thom, D. V. (2019). A refined simple first-order shear deformation theory for static bending and free vibration analysis of advanced composite plates. *Materials*, *12*(15), 2385.

Nikbakht, S., Kamarian, S., and Shakeri, M. (2019). A review on optimization of composite structures Part II: Functionally graded materials. *Composite Structures*, 214, 83-102.

Noorı, A. R., Aslan, T. A., and Temel, B. (2020). Static analysis of FG beams via complementary functions method. *European Mechanical Science*, *4*(1), 1-6.

Noori, A. R., Aslan, T. A., and Temel, B. (2021). Dynamic analysis of functionally graded porous beams using complementary functions method in the Laplace domain. *Composite Structures*, 256, 113094..

Özmen, U., and Özhan, B. B. (2025). Mechanics of functionally graded beams: analytical. computational. and experimental analyses. *International Journal of Mechanics and Materials in Design*, 1-14.

Pradhan, K. K., and Chakraverty, S. (2013). Free vibration of Euler and Timoshenko functionally graded beams by Rayleigh–Ritz method. *Composites Part B: Engineering*, 51, 175-184.

Rahmani, F., Kamgar, R., and Rahgozar, R. (2022). Optimum material distribution of porous functionally graded plates using Carrera unified formulation based onisogeometric analysis. *Mechanics of Advanced Materials and Structures*, 29(20), 2927-2941.

Rasooli, H., Noori, A. R., and Temel, B. (2024). Static analysis of functionally graded porous beam-column frames by the complementary functions method. *In Structures* (Vol. 62, p. 106136). *Elsevier*.

Shahba, A., Attarnejad, R., Marvi, M. T., and Hajilar, S. (2011). Free vibration and stability analysis of axially functionally graded tapered Timoshenko beams with classical and non-classical boundary conditions. *Composites Part B: Engineering*, *42*(4), 801-808.

Shooshtari, A., and Rafiee, M. (2011). Nonlinear forced vibration analysis of clamped functionally graded beams. *Acta Mechanica*, 221(1), 23-38.

Sina, S. A., Navazi, H. M., and Haddadpour, H. (2009). An analytical method for free vibration analysis of functionally graded beams. *Materials and Design*, 30(3), 741-747.

Sinha, G. P., and Kumar, B. (2021). Review on vibration analysis of functionally graded material structural components with cracks. *Journal of Vibration Engineering and Technologies*, 9, 23-49.

Su, H., Banerjee, J. R., and Cheung, C. W. (2013). Dynamic stiffness formulation and free vibration analysis of functionally graded beams. *Composite Structures*, 106, 854-862.

Suresh, S. (1997). Modeling and design of multi-layered and graded materials. *Progress in Materials Science*, 42(1-4), 243-251.

Şimşek, M. (2010). Fundamental frequency analysis of functionally graded beams by using different higher-order beam theories. *Nuclear Engineering and Design*, 240(4), 697-705.

Şimşek, M. (2010). Vibration analysis of a functionally graded beam under a moving mass by using different beam theories. *Composite structures*, 92(4), 904-917.

Thai, H. T., and Vo, T. P. (2012). Bending and free vibration of functionally graded beams using various higher-order shear deformation beam theories. *International journal of mechanical sciences*, 62(1), 57-66.

Tsiatas, G. C., and Charalampakis, A. E. (2017). Optimizing the natural frequencies of axially functionally graded beams and arches. *Composite Structures*, 160, 256-266.

Vo-Duy, T., Ho-Huu, V., and Nguyen-Thoi, T. (2019). Free vibration analysis of laminated FG-CNT reinforced composite beams using finite element method. *Frontiers of Structural and Civil Engineering*, 13, 324-336.

Wattanasakulpong, N., and Ungbhakorn, V. (2012). Free vibration analysis of functionally graded beams with general elastically end constraints by DTM. *World Journal of Mechanics*, 2(6), 297-310.

Weaver Jr, W., Timoshenko, S. P., and Young, D. H. (1991). Vibration problems in engineering. *John Wiley and Sons*.

Youzera, H., Meftah, S. A., Selim, M. M., and Tounsi, A. (2022). Finite element method for axial and bending coupling effect on free vibration response of functionally graded beams under thermal environment. *Mechanics of Advanced Materials and Structures*, 29(27), 6436-6450.

RESUME

Personal Information

Surname, name : Kanoua, Majed

Education

Degree	Education Unit	Graduation Date
Master		
Bachelor		
High School		

Work Experience

Year	Place	Title

Foreing Language

Publications

Hobbies